THESIS FOR THE DEGREE OF DOCTOR OF PHILOSOPHY

Towards an understanding of surface hydrophobization of paper
Exploring the effect of polymer nanoparticles, starch, ionic strength and process parameters

FRIDA ISELAU

Department of Chemistry and Chemical Engineering

CHALMERS UNIVERSITY OF TECHNOLOGY

Göteborg, Sweden 2017

Towards an understanding of surface hydrophobization of paper - exploring the effect of polymer nanoparticles, starch, ionic strength and process parameters

FRIDA ISELAU

Department of Chemistry and Chemical Engineering

Chalmers University of Technology

SE-412 96 Göteborg

Sweden

Telephone +46 (0)31-772 1000

Cover illustration:
Water uptake by paper surfaces treated with surface sizing formulations in different aggregated states. The formulation that gives higher water uptake is in a low aggregated state and the one that gives lower water uptake, and thus better surface hydrophobization, is more aggregated.

Towards an understanding of surface hydrophobization of paper - exploring the effect of polymer nanoparticles, starch, ionic strength and process parameters

FRIDA ISELAU
Department of Chemistry and Chemical Engineering
Chalmers University of Technology

ABSTRACT

Paper materials are cost effective and lightweight, they can easily be recycled and their use as an alternative to plastics is advantageous from an environmental and sustainability perspective. However, competing with plastics for packaging applications is a challenge for cellulosic products. The material needs to be strong and stiff also when exposed to liquids or moisture during transportation and storage. To achieve this for paper materials, which are intrinsically hydrophilic due to the nature of the cellulose, they need to be hydrophobized.

In the paper industry the hydrophobization process is referred to as *sizing* and sizing can be achieved in two ways: adding the hydrophobic compound to the pulp (internal sizing) or on the formed paper surface (surface sizing). Recent development in paper hydrophobization has been towards surface sizing since this method gives better retention of the hydrophobic compound and is also more effective on recycled fibers. There is a plethora of surface sizing products and these products are very efficient in making the paper surface more water resistant, but there is a lack of fundamental knowledge on *how* they work.

The type of surface sizing products studied in this thesis is hydrophobic nanoparticle suspensions and four different particle types have been explored. They have the same polymeric core but different surface charges and chemistries. In the surface sizing application, the suspension is mixed with a starch solution where the starch is added to increase the surface strength of the paper. However, in this thesis it is shown that the starch can have a more active role in controlling the degree of hydrophobization. In the study of the colloidal systems it was found that cationic particles form aggregates with the starch and by maximizing this aggregation a paper surface takes up significantly less water. The aggregation behavior was thoroughly studied and the aggregation could be tuned by amylopectin content, temperature and time. An increased ionic strength had a pronounced effect on the electrosterically stabilized aggregates. Larger aggregates were formed at intermediate ionic strength and when the ionic strength was high enough the system collapsed and large flocs were formed. Both these effects were detrimental for the performance.

In the surface sizing procedure the particle/starch mixture is applied on the paper surface and the liquid penetrates into the paper matrix due to external pressure and capillary forces. The distribution of the hydrophobic polymer on and in the paper was evaluated with time of flight secondary ion mass spectroscopy (TOF-SIMS). The surface distribution did not correlate with the water uptake results, indicating that it is not merely the outermost surface that needs to be hydrophobized in order to have a sufficiently low water uptake. Cross-section analyses revealed that a deeper penetration of the nanoparticles was needed to achieve a water resistant paper.

Keywords: Surface sizing, paper hydrophobization, aggregation, nanoparticles, starch, ionic strength, temperature, charge ratio, kinetics, penetration.

List of publications

This thesis is based on the work presented in the following publications, referred to by Roman numerals (**I-V**) in the text.

I. **Role of the aggregation behavior of hydrophobic particles in paper surface hydrophobation**
Frida Iselau, Per Restorp, Mats Andersson, Romain Bordes
Colloids and Surfaces A: Physicochemical and Engineering Aspects, 2015, **483**, 264-270.

II. **Competitive adsorption of amylopectin and amylose on cationic nanoparticles: a study on the aggregation mechanism**
Frida Iselau, Tuan Phan Xuan, Aleksandar Matic, Michael Persson, Krister Holmberg, Romain Bordes
Soft Matter, 2016, **12**, 3388-3397.

III. **Formation and relaxation kinetics of starch-particle complexes**
Frida Iselau, Tuan Phan Xuan, Gregor Trefalt, Aleksandar Matic, Krister Holmberg, Romain Bordes
Soft Matter, 2016, **12**, 9509-9519.

IV. **Surface treatment by hydrophobic particles: Influence of starch and ionic strength**
Frida Iselau, Krister Holmberg, Romain Bordes
ACS Sustainable Chemistry & Engineering, 2017, **5**, 6107-6115.

V. **Parameters influencing the surface sizing performance**
Frida Iselau, Kerstin Malmborg-Nyström, Krister Holmberg, Romain Bordes
Manuscript submitted to *Nordic Pulp and Paper Research Journal.*

Contribution report

I. Responsible for all experimental work and the data analysis. Responsible for writing the manuscript.

II. Responsible for all experimental work and the data analysis, except for the DLS and SAXS analyses. Responsible for writing the manuscript.

III. Responsible for all experimental work and the data analysis, except for the DLS and SAXS analyses. Responsible for writing the manuscript.

IV. Responsible for all experimental work, except for the surface sizing trials, and the data analysis. Responsible for writing the manuscript.

V. Responsible for planning and evaluating the experimental work and for the data analysis. Responsible for writing the manuscript.

Related publication not included in the thesis:

Towards a mechanism for surface hydrophobization of paper
Frida Iselau, Krister Holmberg and Romain Bordes
Conference proceedings from TAPPI PaperCon 2017

1   TABLE OF CONTENTS

1 INTRODUCTION

Paper products have been a natural part of our daily life since modern paper making started with the development of the Fourdrinier machine,[1] a continuous paper machine that allowed paper making in large scale. The Fourdrinier machine was patented in 1807 and since then paper manufacturing has seen vast developments leading to the variety of paper-based materials that we use today. In recent years the manufacturing process has also integrated the environmental dimension towards more eco-friendly production routes. This fits the image of paper as a material for the future. Paper products are made from a renewable resource and can be recycled many times and eventually the paper waste can generate energy when burned.

It all started almost thousand years ago when the Chinese invented the paper making process.[2] Before that time the ancient Egyptians, Greeks and Romans already had made writing materials from papyrus, hence the name "paper". Today the world production exceeds 400 million tons of paper a year[3] and the paper making process is surprisingly generic despite the versatile paper products that are produced. Variations in the raw material; cellulosic fibers from wood, is of course one parameter that influences the characteristics of the paper produced. Moreover, the paper chemistry together with the choice of additives allows tuning the properties of the paper. When used for communication, like newspapers and magazines, a strong paper with excellent printability is needed. Tissue and household paper should be soft and water absorbent, yet remain strong when wetted by water. A cardboard box should be water resistant in order to withstand various storage conditions such as moist and liquid exposure without losing its strength or shape.

Packaging is a growing market for the paper industry, especially as more goods are transported across the planet. A paper packaging material has many advantages over plastics: it is lightweight, cost effective and made from a renewable source. However, due to the intrinsic hydrophilic character of the cellulosic fibers, packaging paper grades need to be hydrophobized to reduce penetration and wetting by water. The process of making a surface more hydrophobic is referred to as *hydrophobation* or *hydrophobization*. Both terms are used in the literature; however, the trend goes towards using the term *hydrophobization* and, following that trend, the term *hydrophobation*, which was used in the first papers included in this thesis was subsequently changed to *hydrophobization*.

Surface hydrophobization is not needed only for packaging applications. To achieve good printability the paper surface needs to be hydrophobized in order to avoid ink feathering.[4]

In the paper manufacturing industry the hydrophobization treatment is frequently referred to as sizing.[5] If a hydrophobic compound is added to the pulp the process is referred to as internal sizing, and when the hydrophobic compound is applied on the paper surface it is called surface sizing.[6]

This word, sizing, used from historical times, is odd as its meaning is not straightforward. According to the literature the word "sizing" has three plausible origins.[5]

- Size could come from a word for glue because the first sizing method was based on glues. In Swedish and in French the word for sizing is still the word for "gluing"; in Swedish it is called "limning".
- Sizing might come from a test where a stack of papers was put in water and afterwards the increase in size due to water uptake was measured.
- The word "size" could stem from the old Latin verb "assidere". Early Italian papermakers called the procedure "assisa" which can have been modified to "sisa" and then to "size". It means "set in place."

Historically, the first sizing method was surface sizing. It was achieved by wetting the handmade paper sheet through a pond containing the surface sizing ingredients. With this method, there was no mechanical tension affecting the paper's durability. Later, when the paper machines were introduced, the tension on the paper web going through the machine was significantly increased and therefore the paper web often broke due to too high water uptake in the size pond. To solve this problem internal sizing was developed.

In the internal sizing procedure the pulp is treated with a hydrophobic compound, rendering the whole paper matrix more hydrophobic. Internal sizing is typically done by adding hydrophobic, reactive compounds like alkyl ketene dimer (AKD) or alkenyl succinic anhydride (ASA) to the pulp. These compounds react with the hydroxyl groups of the cellulosic chains, forming covalent bonds and rendering the fiber surfaces more hydrophobic.[7-10] The efficiency of the internal sizing process depends on different factors and the procedure suffers from various shortcomings. For instance, it is important to have good retention of the internal sizing agent, i.e. the compound must be retained in the pulp and not be drained off with the recirculating water flow. This is essential since both AKD and ASA are susceptible to hydrolysis and will lose their reactivity if the residence time is too long. Therefore the use of an efficient retention aid is crucial and the pH needs to be on the neutral/basic side in order to avoid hydrolysis. A high filler and/or fines content, as for example in fine paper and recycled paper grades, is detrimental for internal sizing since the hydrophobizing agent is then adsorbed on the small particles/fibers and not on the main fibers. With a high content of fines a higher dosage of internal sizing agent is therefore needed.

Surface sizing is, as the name implies, a surface treatment of the formed paper sheet. The meaning of the term surface sizing is broad and can involve use of various components to achieve the desired paper properties.[2] Commonly, starch is applied on the paper surface in order to enhance the paper stiffness by forming a film on the paper surface that creates strong hydrogen bonds with the cellulose fibers.[11] The applied starch can also reduce the water penetration rate by filling the surface voids in the paper sheet.[12] In this thesis surface sizing refers to a hydrophobization method where a hydrophobic compound is applied on the paper surface. By this procedure the hydrophobic compound is first mixed with the starch solution and the mixture is subsequently applied on the paper surface at the dry-end of the paper machine.[6] (See Figure 1.1).
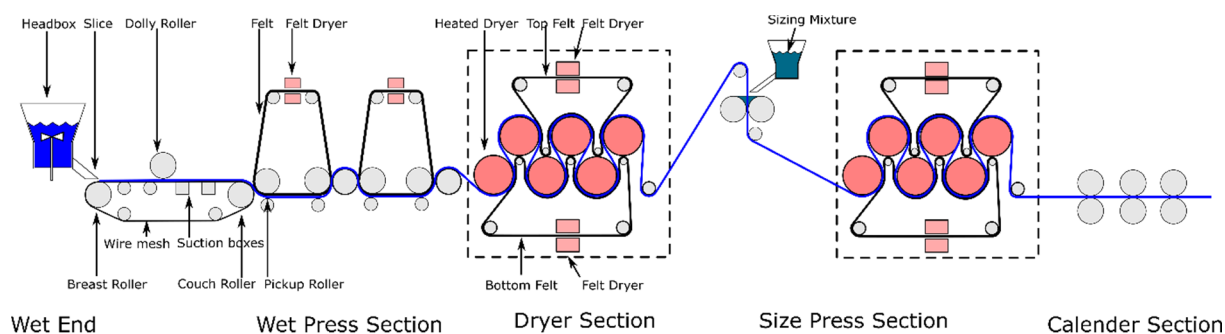
Figure 1.1. *Illustration of the paper making process (adapted from "Diagram showing the sections of the Fourdrinier machine" created by Egmason, available under a Creative Commons Attribution 3.0 license.)*

In the surface sizing procedure pressure is applied and the paper is usually heated to above the glass transition temperature of the polymer in order to promote coalescence of the particle layer.[13] There are different techniques to industrially apply the particles on the surface of the paper, the most important being puddle press and film press.[12, 14] For both techniques, the paper is first exposed to the particle/starch suspension to allow liquid absorption and adsorption to take place, and then, exposed to an external pressure, the press step. This is followed by the drying step. Figure 1.2 shows a schematic description of surface sizing at laboratory scale.
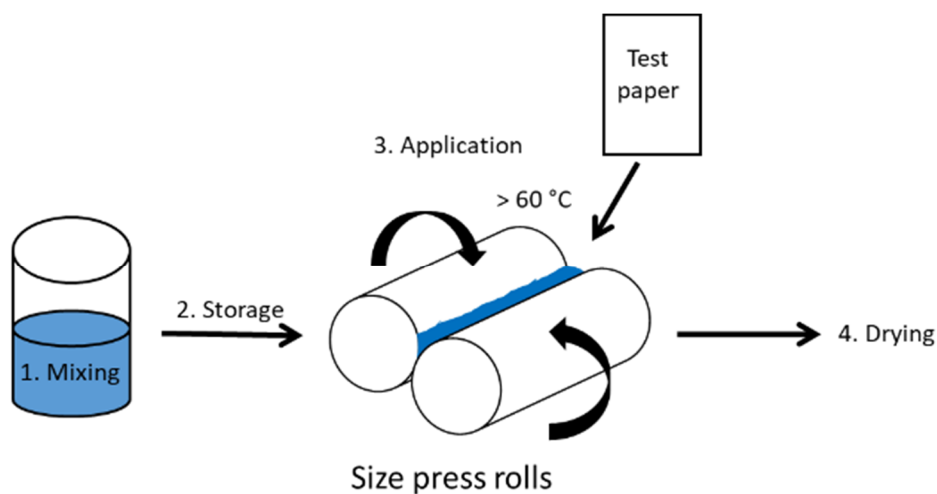
Figure 1.2. *A schematic representation of the surface sizing procedure.*

In this surface sizing application the paper material is typically treated with a suspension of hydrophobic polymer particles in a starch solution.[12, 15-18] The hydrophobic polymer particles, typically a styrene-acrylate based copolymer stabilized by amphiphiles of different nature,[13, 17, 19, 20] render the paper surface hydrophobic.[12, 15, 19, 21, 22]

For technological, economic and environmental reasons there is currently a shift from internal sizing to surface sizing.[23] In surface sizing the hydrophobic compound is mainly present at the paper surface, where they are primarily needed, allowing a significant reduction of the amount of chemicals used in the hydrophobization process. Surface

sizing has the additional advantage of having efficient retention[11, 12, 16, 18, 24] which is beneficial both from an economic and a process runability point of view.[12] Technical reasons also favor surface sizing over internal sizing. For instance, for recycled paper, where the composition may vary a lot, efficient internal sizing is often difficult to achieve.[24]

Surface sizing polymer suspensions are widely used in the paper making industry today and there is a variety of grades differing in particle size, colloidal charge and chemical composition. Although the various grades are known to be very efficient there is a lack of fundamental knowledge of *how* these products work. Hence, a more knowledge-based development of surface sizing products is essential in order to obtain products that in the future will be able to compete with other packaging materials in new applications. The first step towards such a knowledge-based development is to gain a deeper understanding of the fundamental principles that govern the surface sizing performance.

The surface sizing performance for four different particle types, all representative of products commonly used in paper mills, was explored. The particles consist of the same hydrophobic polymer core but with different stabilizers. At an early stage of this thesis work, it was seen that the relationship between the colloidal behavior of the particles and their efficiency had not been explored. Particle characterization and evaluation of the surface sizing effect of the different particle types are described in **Paper I**, where also an initial interaction study between the particles and starch is presented. **Paper II** further explores the interactions between the surface sizing components and an aggregation mechanism is proposed. The kinetics of the aggregation was investigated by light scattering techniques and described utilizing the Kohlrausch-Williams-Watts function (**Paper III**). The interactions introduced in **Paper I** and further explored in **Paper II** and **Paper III** were correlated to an improved efficiency in surface hydrophobization when optimal conditions were applied as described in **Paper IV**. Also demonstrated in **Paper IV** is the influence of an increased ionic strength on both aggregation and surface sizing performance. The final paper included in this thesis, **Paper V**, makes a holistic evaluation of which material properties and process parameters that influence the surface sizing performance. Also included in this thesis are results from a TOF-SIMS study exploring the distribution of the hydrophobic polymer on the paper surface and in a cross-section of the paper. The results from this study will be part of a future publication.

The conclusions from this thesis work will hopefully give new insights and a deeper understanding of the mechanism of surface sizing, towards a knowledge-driven process optimization.

2 OBJECTIVES

The aim of this thesis is to gain deeper understanding of the fundamental principles that govern surface sizing. It has been said that there are as many variations of surface sizing as there are paper mills in the world; however, the basic principles of surface sizing are generic. The scheme of the surface sizing procedure shown in Figure 1.2 can be divided into four steps:

1. Mixing of components
2. Storage of mixture
3. Application
4. Drying

Together, these steps will lead to a hydrophobized paper surface and it is therefore important to evaluate the whole process in order to identify the crucial parameters for achieving the optimal surface sizing effect. In this thesis all four steps are considered and their interconnections are explored.

3 ANALYTICAL TECHNIQUES

The complexity of the systems studied in this work is reflected by the diversity and the broad range of analytical techniques employed. Scattering techniques give information about the overall behavior of the colloidal system with emphasis on aggregation behavior, size of the particles and aggregates, and surface charge.

One of the principles of surface sizing is to achieve a hydrophobic paper surface by applying hydrophobic nanoparticles. The degree of hydrophobization can be evaluated by the means of reduction of water uptake in a Cobb test or by contact angle measurements.

When the particle suspension has been applied on a paper surface its distribution on and in the paper matrix has been characterized with TOF-SIMS.

3.1. TURBIDITY

When light passes through a particle suspension the incoming beam is scattered due to interactions with the matter. When the particle size is smaller than the incoming wavelength of the light the turbidity increases with particle size.[25] Turbidity can be used for monitoring size growth due to aggregation, however not quantitatively. A UV/Vis spectrophotometer can be used for turbidity measurements where incoming light in the UV and visible spectra, from 200-800 nm, is illuminating the sample. The intensity of the transmitted light is monitored and its decrease is the results of the presence of aggregates and of their size.

3.2. DYNAMIC LIGHT SCATTERING

When a radiation beam is illuminating a sample, the beam is scattered. The scattering pattern is the result of the inhomogeneity of the sample. The scattered beam is monitored by detectors and the intensity of the scattered beam as a function of the angle of detection is measured. Light scattering provides a non-invasive measurement of macromolecules and particles in solutions or dispersions. From scattering measurements information about size, molar mass, radius of hydration, radius of gyration and form factor can be extracted. The theory of Rayleigh states that the scattering intensity is proportional to the power of six of the particle size, meaning that the larger the particle the higher is the scattering intensity.[26]

In a dispersion, the solvent will have an impact on the particles causing them to move, the so-called Brownian motion. Dynamic light scattering, DLS, is a scattering technique where the time-dependent fluctuation in the scattering from the movement of particles due to Brownian motion is monitored. The fluctuation is correlated to the diffusion rate of the particle in the solvent and the diffusion rate is in turn correlated to the hydrodynamic radius of the particle. The hydrodynamic radius (R_H) can be calculated from the average diffusion coefficient (D) using the Stokes-Einstein equation (Eq. 1):

$$D = \frac{kT}{6\pi\eta R_H} \qquad \text{(Eq. 1)}$$

Where η is the viscosity, k is the Boltzmann's constant and T is the absolute temperature.

The radius of hydration, R_H, that is obtained from DLS is for a sphere always larger than the radius of gyration, R_G, obtained from static light scattering measurements. The diffusion coefficient obtained from the equation above is the so-called Z average particle size. The Z average calculated particle size arises from the cumulant mean and is regarded as the primary and most stable value. It is therefore common to report the Z average as the value for the hydrodynamic radius. However, the intensity-weighted value is sensitive to larger sizes and by employing Mie theory the intensity distribution can be calculated into a volume or number size distribution that is less sensitive towards larger sizes.

3.3. ELECTROPHORETIC MOBILITY AND ζ POTENTIAL

A charged particle suspension has a distribution of counter-ions surrounding the particle surface. Close to the surface the counter-ions are strongly bound and this is defined as the Stern layer. Outside the Stern layer there is still a higher ion concentration compared to the bulk but the ions are less firmly bound to the particles. This layer is called the diffuse layer. When a voltage is applied to a particle suspension an electric field is created and the particles are attracted to the electrode of opposite polarity. The particle velocity in this electric field can be measured and from this the electrophoretic mobility, μ_e, can be calculated from the relation $\mu_e=v/E$, where v is the velocity and E is the applied electric field.[27] The velocity is measured by electroacoustic or laser Doppler electrophoresis techniques. The detection for the instrument used in this study was laser Doppler electrophoresis which utilized the Doppler effect, i.e. that a moving object will induce a phase shift in frequency.[28] By comparing the frequency of the scattered light with incoming light frequency, the velocity can be calculated. The electrophoretic mobility depends only on the amount of charge carried by the particle and not on the particle shape or size.[29]

When an external voltage is applied to the particle suspension, the ions bound to the particle surface will move along with the particle. At a specific distance from the particle surface, inside the diffuse layer, there is a limit where the ions no longer follow the particle's movement. This is called the slipping plane. The potential at this border is defined as the ζ potential and can be calculated by the Smoluchowski formula where the ζ potential is obtained from the viscosity of the solution, the dielectric constant and the electrophoretic mobility.[27] The ζ potential therefore reflects the effective particle charge and is the potential in the electrical double layer that exists between the particle surface and the surrounding medium, often water. The ζ potential is dependent on solution conditions such as pH and ionic strength, and the ζ potential measurements should preferably be performed with a constant background electrolyte concentration.

3.4. COBB TEST

The Cobb test is a water absorptiveness measurement on sized paper according to TAPPI standard method 441.[30] In this test the water absorptiveness, i.e. the Cobb value, is defined as the mass of water absorbed in a specific time by 1 m^2 paper under 1 cm of water and given in the unit g/m^2. The exposure time is often 60 seconds but for specific requirements also longer times can be employed, for example Cobb1800 which corresponds to an exposure time of 1800 seconds. The lower the Cobb value the better

is the water resistance of the tested surface. A Cobb value below 30 g/m^2 is usually regarded as a sufficiently hydrophobized surface.

3.5. CONTACT ANGLE

Wetting of a solid surface is attributed to an unbalance in surface forces and was defined by Thomas Young in 1805.[29] To what extend a liquid is able to wet a surface depends on the properties of both the liquid and the surface. When a drop of a liquid is deposited on a solid surface, adhesive forces will strive to spread the drop on the surface in order to decrease the surface free energy of the solid surface. The interfacial tensions of the liquid to the air and to the solid will at the same time strive to minimize the spreading by the act of cohesive forces. Figure 3.1 illustrates wetting of a surface by a water drop.
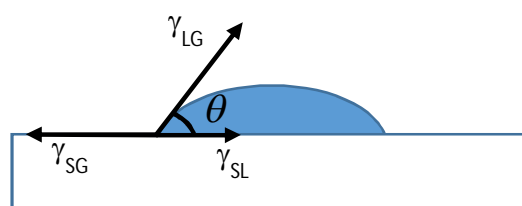

Figure 3.1. *Forces acting on a water drop on a solid surface.*

These forces will be balanced when the spreading of the drop has reached equilibrium.[31] The relation that describes the forces acting on the drop is known as Young's equation (Eq. 2) and is defined as:

$$\gamma_{SG} = \gamma_{SL} + \gamma_{LG} cos\theta \qquad (\text{Eq. 2})$$

Where γ_{SG} is the surface free energy of the solid, γ_{SL} the interfacial tension between the solid and the liquid and γ_{LG} the surface tension of the liquid. The contribution to the cohesive force from the liquid surface tension is angular dependent. This angle, θ, is defined as the contact angle. A more hydrophobic surface has a higher contact angle compared to a hydrophilic surface where wetting is favored and thus the angle of contact is low.

Young's equation assumes a smooth, homogenous, isotropic, insoluble and non-reactive surface.[32] A paper surface is porous and structured, it has a heterogeneous composition due to the addition of filler and AKD (for fine paper) and residues from processing and the wood origin (for liner). In addition, the water drop will penetrate into the paper surface due to capillary forces causing a change in contact angle with time. Nevertheless, despite all these exceptions from the requirements of Young's equation, the sessile drop method can give important and valuable information provided that the data is evaluated with caution.

3.6. TOF-SIMS

Time of flight secondary ion mass spectroscopy, TOF-SIMS, is a technique that has been described as chemical microscopy.[33] Detailed chemical information can be achieved from mass spectra that are obtained from the outermost part of a surface. This is referred to as *static SIMS*.[34] In SIMS, the surface of interest is bombarded with primary ions, for example Ga$^+$, Ar$^+$ or Cs$^+$. These ions will give rise to desorption of

fragments from the surface. Most of them will be neutral but it is only the secondary ions that form that will be analyzed in the mass spectrometer. SIMS measurements are destructive because the secondary ion fragments are removed from the surface due to the ion bombardment. However, by utilizing a low dose of primary ions, less than 1 % of the atoms at the top surface layer will be affected and the impact will be randomly distributed. With SIMS both positive and negative ions can be analyzed and all types of molecular species that are vaccuum compatible can be quantified.[35]

TOF-SIMS is a type of static SIMS instrument. The advantages of TOF-SIMS are high sensitivity, high mass resolution, unlimited mass range and accurate mass determination.[35] In a time-of-flight measurement the ions of interest are accelerated with the same kinetic energy, E, and the time it takes for the ion to travel a known distance before reaching the detector is measured. The velocity of the ion depends on the mass to charge ratio, m/z. This means that heavier ions travel slower than lightweight ions. The flight time is thus proportional to the square root of the ion mass, and the flight times for the emitted secondary ions generate the mass spectrum.[34]

4 MATERIALS AND METHODS

4.1. MATERIALS

4.1.1. The hydrophobic nanoparticles

The hydrophobic, polymeric nanoparticles that were used throughout this thesis work are similar in composition to commercial available surface sizing products used in the papermaking industry today. This is an important aspect since the aim of the project is to contribute to the understanding of the surface hydrophobization process at the paper mill. However, in order to have control over the composition and to vary the surface charge in a controlled manner, the different particle types that have been employed throughout this thesis work were synthesized specifically for this project.

The hydrophobic nanoparticles studied in this thesis are labelled "SP+", "SPA+", "SPA-" and "SP-" where SP stands for Size Press which is the application and the sign describes the net surface charge of the particles. A, stands for Amphoteric and means that SPA- and SPA+ carry both cationic and anionic charged groups. All particle types have the same hydrophobic core, consisting of a co-polymer of styrene, n-butyl acrylate and tert-butyl acrylate but they have different types of stabilizer. SP+ has a synthetic, cationic stabilizer while SPA-, SPA+ and SP- particles are stabilized by an oxidized, degraded starch, which in the case for SPA- and SPA+ are also cationized. The composition of the particles is the same for all particle types; 60 wt. % hydrophobic polymer in the core and 40 wt. % stabilizer.

The SP+, SPA- and SP- particles were synthesised as described in **Paper I**. The net cationic, starch-based particle type SPA+, utilized in **Paper V,** was synthesized in the same way as the starch-based SPA- and SP- with the exception that a more cationized starch was used for the SPA+ synthesis. The radical polymerization was carried out as an emulsion polymerization in the presence of the stabilizer (degraded starch or synthetic copolymer). The polymerization was initiated by hydrogen peroxide in presence of iron-(II)-sulphate that acts as a catalyst for formation of radicals. To control the molecular weight, dodecanethiol was used as a chain transfer agent. The particle synthesis was repeated to assess variations in the synthesis routine. The reproduced particle batches were found to have similar properties and the overall behavior was the same. A schematic view of the particles is shown in Figure 4.1.
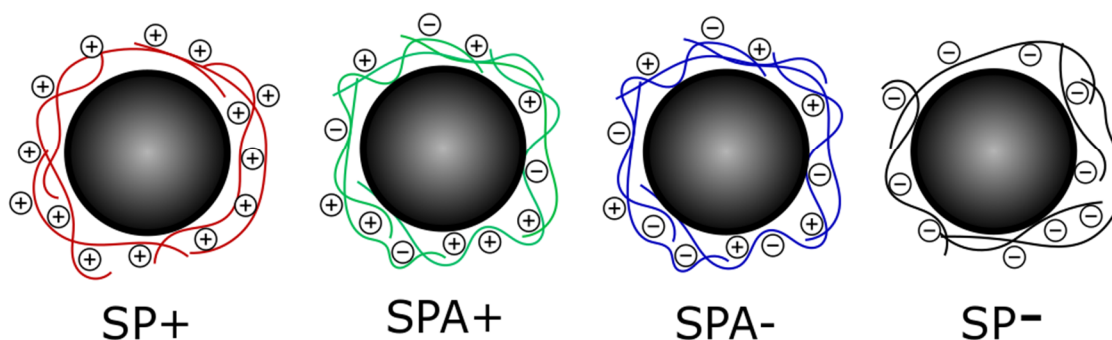
Figure 4.1. *Schematic illustration of the particle composition. Colloidal stability is achieved by a cationic, amphoteric or anionic stabilizer, as illustrated in this figure.*

In one of the studies described in **Paper III**, amidine latex particles (AL110) from Invitrogen (Basel, Switzerland) was used.

4.1.2.   Starch

Starch is a biopolymer with glucose as the repeating unit connected through α (1→4) glycosidic bonds.[36] The polyanhydroglucose chain can form two types of polymers: amylose and amylopectin. The amylose chains are linear and relatively short while the amylopectin is highly branched and of high molecular weight. An illustration of the starch components and their structure is shown in Figure 4.2.
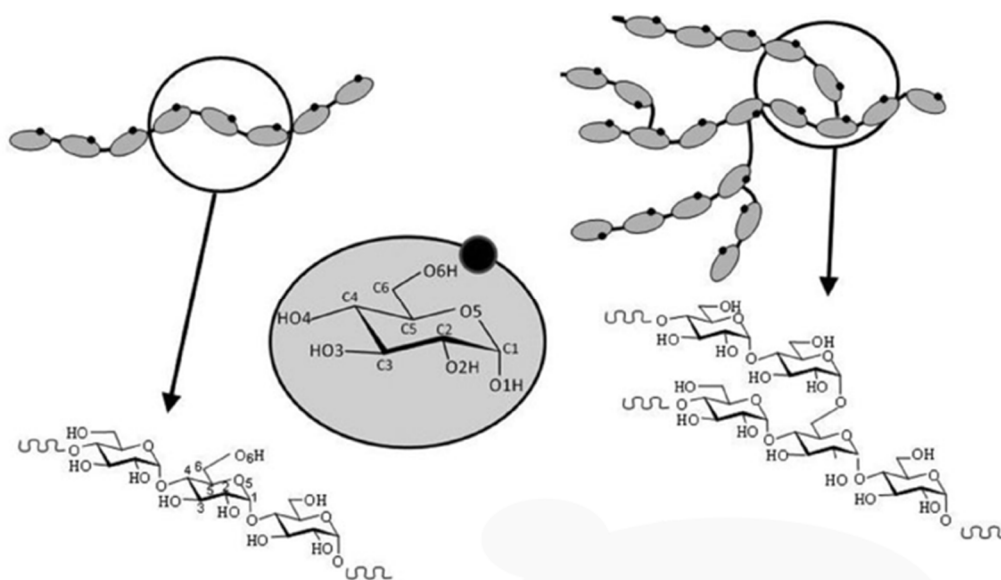

Figure 4.2. *Schematic description of the starch components amylose (linear) and amylopectin (branched). (Reprinted with permission from Wiley Materials. The original is found in "The molecular structures of starch components and their contribution to the architecture of starch granules: A comprehensive review" by Serge Peréz and Eric Bertoft, Starch 2010, 62, 389-420.)*

11

Different types of native starch have different proportions of amylopectin and amylose in the granules.[37] The composition of regular potato starch is typically 20 wt. % amylose and 80 wt. % amylopectin.[37] In contrast, waxy starch contains only amylopectin. Native starch has a very high average molecular weight and gives rise to high viscosity when dissolved in water. Therefore the starch used for surface sizing is degraded prior use in order to decrease the molecular weight, which leads to reduced solution viscosity. The degradation is done by either oxidative, enzymatic or thermomechanical treatment and depending on degradation method the starch will have somewhat different molecular weight distribution and charge. In this research work, oxidized starch was employed for which the oxidation was done with sodium hypochlorite (NaClO). The process leads to a depolymerization of the starch and at the same time generates carboxylate groups in the starch.[38] Thus, oxidized starch will have lower molecular weight and carry an anionic charge, which will be pH dependent. The charge density depends on the amount of NaClO added, and typical values of degree of substitution (carboxyl groups) are 0.03-0.05 mol/mol for oxidized potato starch. The structure of oxidized starch is schematically shown in Figure 4.3.
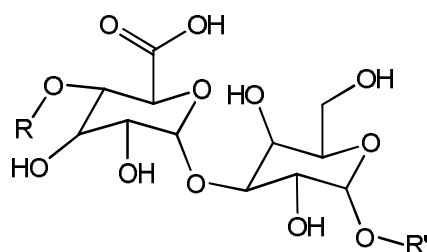

Figure 4.3. *Structure of oxidized starch.*

The starch mainly used in this research work was an oxidized regular potato starch from Avebe, The Netherlands. For some of the studies the influence of amylopectin and amylose was investigated and then a second starch type, an oxidized waxy potato starch, also from Avebe, was used. Both starch powder types were used as received.

4.1.3.   The test papers

As test papers, a liner grade and a fine paper grade were used in this study. The liner was a 100 % recycled, unbleached, not internally sized paper grade with a basis weight of 140 g/m^2. This means that the liner grade contains residues of lignin and rosins that render the paper slightly hydrophobic, which is needed in the size press to avoid disintegration. The fine paper grade consisted of 100 % virgin fibers from birch with a calcium carbonate filler content of 16-18 wt. % and 0.5 wt. % cationic starch for mechanical strength enhancement. The basis weight was 80 g/m^2. The fine paper grade was internally sized with alkyl ketene dimer (AKD) in order to withstand the forces in the size press without disintegrating.

4.2. ANALYTICAL METHODS

The complexity of the materials studied in this thesis is reflected in the many analytical techniques that have been employed to explore their properties. The analytical methods used are in some cases complementary and used for confirming the observed results. Differences in length scales, from nano to micro scale have also invoked a diversity in analytical techniques. The analytical methods used in this thesis work are listed below together with a short description, for more details, see the **Papers I-V** at the end of this thesis.

4.2.1. Methods for colloidal studies

Turbidity – turbidity measurements were performed using a UV/Vis spectrophotometer. The value of the absorbance at 400 nm was used as a measure of the turbidity for the studies of the influence of starch and salt on the particle suspensions.

ζ **potential** – was measured using a Malvern Nano instrument where the ζ potential was derived from the electrophoretic mobility by laser Doppler electrophoresis. The ζ potential reflects the effective particle charge and was used both for determining the charge of the particles and the reduction of particle charge due to aggregate formation by the adsorption of starch.

MALS – A multi angle light scattering (MALS) instrument, ALV/CGS-8F, was employed for dynamic light scattering measurements on SP+/starch complexes.

PCD – a particle charge detector (PCD) from CAS Charge Analyzing System (AFG, Analytic GMBH) was used for determine the colloidal surface charge of the fiber suspensions and starch solutions. This is an electrokinetic technique where the charge distribution is determined by measuring the streaming potential.[39, 40] The amount of surface charge is determined by the titration of the sample with a titrant carrying the opposite charge and the amount of titrant required for charge neutralization on a macroscopic level is used for calculating the charge density.

SAXS- Small Angle X-ray scattering (SAXS) was carried out at the I911-4 beamline of the MAX-Lab synchrotron in Lund. With SAXS the radius of gyration and the internal structures of the nanosized aggregates were investigated.

SEC-MALS/RI – An instrumentation for size exclusion chromatography with multiple angle light scattering and refractive index detection (SEC-MALS/RI) from Wyatt Technology was used for determining the molecular weight of the starches and for determining the depleted fraction of the starch in the aggregation study.

Rheology – A Brookfield DV-III Ultra Viscometer equipped with a UL adapter was employed to measure the viscosity of the starch solutions and also how the starch solution viscosity was affected by increased ionic strength.

Laser diffraction – A MasterSizer Microplus instrument from Malvern was used for determining the size and shear sensitivity of the formed flocs in the salt study.

4.2.2. Particle characterization methods

DLS – for determining the particle size and distribution, a Malvern Nano instrument was used for determining the radius of hydration by dynamic light scattering (DLS).

DSC – A differential scanning calorimetry (DSC) instrument from Mettler Toledo was used to determine the glass transition temperature for the different particle types.

Freeze fracture with transmission electron microscope (TEM)* - The samples were prepared by the freeze fracture mica method and then high resolution TEM pictures could be taken. In this method a small amount of a diluted sample was placed in between two mica plates and rapidly frozen in liquid nitrogen. The mica sandwich was split up and the surface now covered by a frozen particle suspension was placed in a holder, still in liquid nitrogen and placed in the vacuum chamber. In the chamber, the temperature was -170 °C to allow water sublimation. The surface was then covered by a platinum layer, 0.8 nm thick, and a 2 nm carbon layer. The carbon layer worked as a support for the thin platinum layer. The reproduction of the sample structure was then studied by TEM. The three particle types SP+, SP- and SPA- at concentrations of 0.05-0.07 wt. % were included in the study.

4.2.3. Paper surface characterization methods

XPS – X-ray photoelectron spectroscopy (XPS), was used to determine the chemical composition of paper surfaces.

SEM – Scanning electron microscopy (SEM) was employed for imaging the paper surfaces in order to investigate the surface structure and coverage of the surface sizing mixture. SEM imaging was also performed on paper surfaces with the tilting angles of 10 ° and -10 ° in order to create 3D reconstructions of the surfaces.

Air permeability and surface roughness – The air permeability and roughness were measured using a Bendtsen equipment where pressurized air is flowed through the paper sheet for determination of air permeability and along the paper surface for the determination of surface roughness.

Fluorescence microscope* – A fluorescence microscope from Zeiss was used for imaging the fluorescence from fluorescent labelled particles. The particle suspension was spin coated on silicon wafers and dried in room temperature or at 80 °C and the fluorescence was captured using the same exposure time in order to compare the fluorescence intensity.

TOF-SIMS* – with time of flight secondary ion mass spectroscopy (TOF-SIMS), the chemical composition of the outermost layer of a surface can be determined. Secondary ion spectra and images were recorded using a TOF-SIMS[5] (ION-TOF, Münster, Germany) with a 30 kV Bi_3^+ primary ion beam. The imaged area size was generally 200 μm x 200 μm with 1024 x 1024 pixels. Three spectra (i.e. three primary ion pulses) were acquired for each pixel. TOF-SIMS was used for investigating the surface coverage and penetration of cationic particles on and in a fine paper sheet. Reference spectra were taken for the paper constituents as well as for SP+. High spatial resolution spectra (with a lateral resolution of approximately ½ μm) were obtained in positive ion mode.

4.2.4. Paper surface hydrophobization evaluation methods

Contact angle – A Fibro DAT system utilizing the sessile drop technique was used for determining the contact angle of water on surface sized paper sheets. The evolution of the contact angle after application up to 60 seconds was monitored and used for investigating the degree of surface hydrophobization.

Cobb60 – The paper's resistance towards wetting was evaluated with the Cobb60 method. This method is a water pick-up test by weight, where 100 mL of deionized water is applied onto a 100 cm^2 area of the paper surface during 60 seconds using a retaining ring that is clamped on top of the paper. After 60 seconds the excess of water is removed and the water uptake is measured as a weight increase of the paper sheet.[13]

*These methods are not included in the papers and are therefore described more in detail here.

5 PROPERTIES OF THE PARTICLES, THE STARCHES AND THE TEST PAPERS

5.1 THE HYDROPHOBIC PARTICLES

In this research work four different particle types have been utilized and their properties have been thoroughly investigated. All four particle types have the same hydrophobic polymer core; a copolymer of styrene and butyl acrylates, but they differ by the type of stabilizer. The particle type called SP+ has a cationic, synthetic polymer as stabilizer. The SPA-/SPA+ types have a cationized, oxidized starch as stabilizer and the SP- type is stabilized by an oxidized starch.

The particles were characterized using several analytical tools as well as imaging techniques. The particle sizes, the ζ potentials and the glass transition temperatures are listed in the Table 5.1 below. The values listed in Table 5.1 are from one set of experiments. In **Paper I** the particle size and Zeta potential for SP+, SPA- and SP- were measured by dilution of the particle suspensions in 1 mM NaCl. Later in the project a salt sensitivity was discovered for SP+, therefore the listed properties in Table 5.1 were determined in Milli-Q water. In **Paper I** the volume size distributions were reported while in the subsequent papers the Z average hydrodynamic radius (R_H) was reported. The particle sizes listed in Table 5.1 are the Z average hydrodynamic radius for all four particle types.

Table 5.1. *Particle properties.*

Particle type	Z average R_H, nm	ζ potential, mV	Tg (°C)*
SP+	25	+46	66.9
SPA+	33	+11	62.4
SPA-	36	-14	62.4
SP-	36	-27	65.7

*The Tg values reported here are from the second heating cycle.

The particles prepared in the presence of the starch-based stabilizers have similar sizes, around 35 nm in radius. The particles prepared with the cationic synthetic emulsifier, SP+, are smaller, with a radius of 25 nm as a result of the higher effectiveness of the emulsifier. The difference in particle size means that the active surface area differs between SP+ and the other particle types. This could influence for example adsorption, heat transfer and mobility.

Regardless of the stabilizer type, the glass transition temperatures obtained are between 62 - 67 °C. This is important since the glass transition temperature of the hydrophobic polymers in the particle core will govern the flexibility of the polymers upon heating which in turn can affect the sizing efficiency and the film forming process.

The effective charge of the particles is reflected by their ζ potential and as expected SP+, prepared with the cationic synthetic stabilizer, has a pronounced positive ζ potential. The ζ potential of SP-, where an oxidized starch was used as stabilizer, is strongly

negative while the degree of cationization of the starch used for SPA- and SPA+ is reflected in their ζ potentials; for SPA+, where a more cationized starch was employed, the ζ potential is net positive while for SPA- it is net negative.

Freeze fracture TEM was employed for imaging the particle types, SP+, SPA- and SP- and the TEM pictures of the particles (Figure 5.1) confirmed the particle sizes determined by DLS. The pictures also revealed a difference in behavior on the slightly anionic charged mica surface for the different particle types. The sample preparation for SP- was more difficult as there was repulsion between the anionic particles and the mica surface and therefore the imaging of SP- was unsuccessful. The cationic particles, SP+, were evenly distributed on the mica surface due to attraction to the surface and repulsion between the individual particles. The amphoteric SPA- showed a more random distribution on the surface.
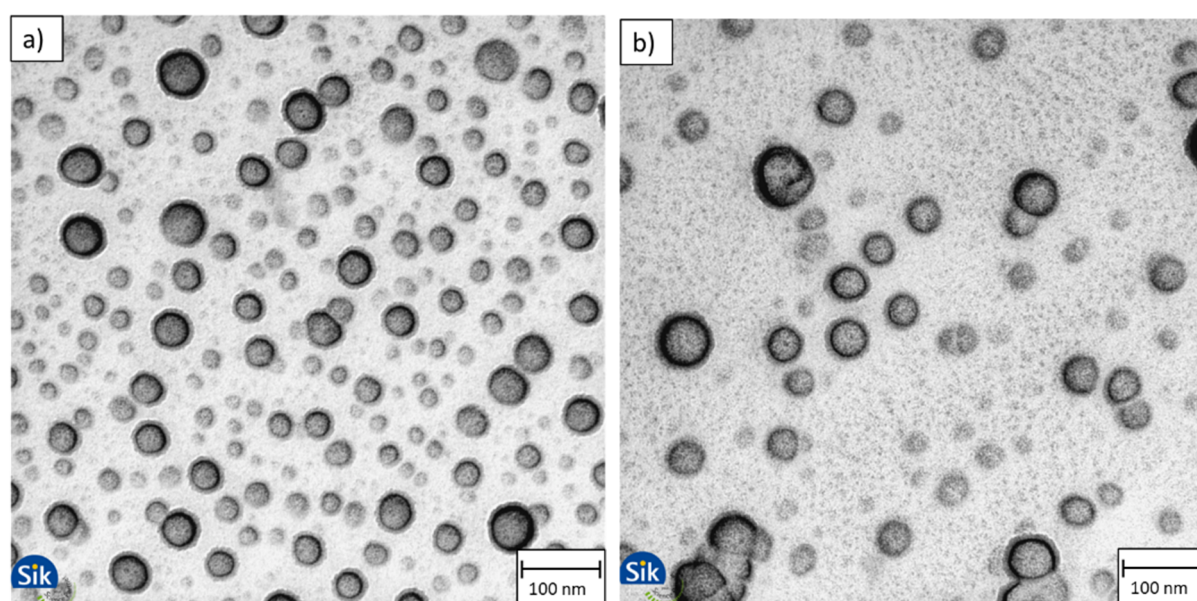

Figure 5.1. *TEM pictures of a) SP+ and b) SPA-, on mica surfaces.*

The radius of gyration, R_G, for SP+ was obtained by SAXS and was determined to 14 nm. The form factor value of $P = 3.8$ showed that the particle presents a rough fractal surface. This can be explained by the core-shell structure of SP+ where the polymeric stabilizer acts like polymer brushes on the surface.[41]

5.2 STARCHES

Starch is used in the surface sizing process to increase the surface strength[14] of the paper and to contribute to paper stiffness.[11] The application of starch on the paper surface will also decrease the rate of water uptake by providing a smoother surface. However, due to its intrinsic hydrophilicity, starch makes the paper surface more prone to adsorb water. For some paper grades it is sufficient to surface size with only starch but in most cases starch in combination with polymer particles is used. Native starch has a too high molecular weight to be handled properly in a paper mill and the starch is therefore always depolymerized before use.

The molecular weight of the starch will influence the surface sizing process by affecting the viscosity of the surface sizing formulation and thus the retention and penetration of the mixture onto and into the paper matrix.[42] The molecular weight and molecular weight distribution of the starches were therefore examined. The oxidized starches that were used in this thesis work are polyelectrolytes with the potential to interact both with the particles and the paper surface, therefore the colloidal charge of the starches was also determined.

Size exclusion chromatography, SEC, is a chromatographic technique that separates the starch in solution with respect of chain lengths, where the longer polymer chains are eluted first. The combination of refractive index (RI) and multiple angle light scattering detectors gives the absolute molecular weight and the molecular weight distribution of the analyzed sample. The results from the SEC analysis are listed in Table 5.2. The waxy starch was less oxidized compared to the regular starch, giving the waxy starch a higher molecular weight and also a somewhat lower anionicity. The polydispersity index, M_w/M_n, for regular starch was higher compared to the waxy starch. This is due to the amylose part of the regular starch since amylose chains have low molecular weight compared to amylopectin. The polydispersity for the waxy starch is due to the natural origin of the polymer and also due to the oxidation process. The RI response for the oxidized starch was in accordance with previous studies where SEC was used for determining the molecular weight distributions of oxidized starch.[43]

Table 5.2. *Properties of the starches.*

Starch type	Colloidal charge, $\mu eq/g$	M_n, kD	M_w, kD	M_w/M_n	R_G (nm)
Regular starch	-180	202	870	4.3	7
Waxy starch	-130	1380	3090	2.2	7

From SAXS measurements the radius of gyration was determined to 7 nm for both the regular and the waxy starch. Since both starch types were found to have the same radius of gyration it was concluded that only the amylopectin fraction was detected by SAXS.

The colloidal charge for the two starches in solution was determined by colloidal charge titration where the anionic starches were titrated with a cationic polymer with a known charge density, in that case polyDADMAC. The colloidal charge was determined to - 180 µeq/g and -130 µeq/g for the regular and the waxy starch respectively. The difference in charge is due to a difference in degree of oxidation as discussed above for

18

the molecular weights. Since the starch has very low scattering intensity the ζ potential could not be determined.

5.3 CHARACTERIZATION OF THE TEST PAPER TYPES

Two types of model papers were used throughout this thesis; one recycled liner grade and one fine paper grade. The recycled liner was an unbleached paper board type that consists of 100 % recycled fibers. The liner grade has thus a very diverse composition and was not internally sized but have some hydrophobic character due to residues of lignin and extractives. The fine paper grade was from a pilot machine and the composition was therefore well-defined. The fine paper was internally sized, which is necessary in order for the thin, hydrophilic paper sheet not to disintegrate during the surface sizing procedure.

5.3.1 Colloidal charge of fiber slurries

The colloidal charge was determined by colloidal charge titration using a particle charge detector, PCD, on a slurry of disintegrated paper. The anionic charge of the liner grade was determined by PCD to be -10 µeq/g. This is lower than has been reported in the literature for pulp slurries[44, 45] but reasonable considering the fact that the liner is constituted of recycled fibers and that the fibers loose some charge during repulping. The anionic charge of the fine paper grade was determined to be -5 µeq/g which is also lower than expected. However, the cationic starch and the filler, calcium carbonate, might contribute to this apparent low colloidal charge. The anionic charge in the fine paper is due to oxidation during pulping. For the recycled liner grade the anionic charge might originate from residues of lignin (oxidized), extractables (fatty acids, resin acids) as well as from processing conditions rendering carboxylic groups on the cellulose.

5.3.2 Chemical composition of the paper surface

The chemical composition of the test paper surfaces as determined by XPS is summarized below (Table 5.3). As comparison, the composition of filter paper made of pure cellulose is included in the table. The fine paper has similar elementary composition as the pure cellulose filter paper except from the calcium content that comes from the calcium carbonate used as filler. The chemical composition of the liner is somewhat different and is due to the residual content of lignin, fatty acid, resins and other compounds.

Table 5.3. *Chemical composition of the two test paper types. Also included in the table is the chemical composition for a filter paper.*

Paper type	Carbon	Oxygen	Calcium	Other
Filter paper	54.7	45.3		
Fine paper	55.7	41.0	3.3	
Liner	66.1	32.3	0.3	1.3

The anionic charge of the fibers determined by the PCD titrations originates only from carboxylic groups since the XPS analyses did not show any sulfur content which rules out the possibility of anionic sulfonate groups contributing to the anionic charge.

5.3.3 Permeability and surface roughness

In Table 5.4 the surface roughness and porosity properties of the liner and the fine paper, determined with air flow techniques, are listed. The fine paper was determined to have larger porosity compared to the liner grade which might seem contradictory since the density of the fine paper was higher. However, what is not captured in this type of porosity measurements using air flow is the impact of the paper thickness. The liner grade has more than twice the thickness of the fine paper and if the porosity is normalized by the thickness the porosity for the fine paper grade would be more than two times lower than the liner grade. The surface roughness measurements determined with air flow, showed that the liner surface was around six times more rough than the fine paper grade.

Table 5.4. *Properties of the fine paper and the liner.*

Paper type	Porosity (ml/min)	Roughness (ml/min)	Grammage (g/m^2)	Thickness (µm)	Density (g/cm^3)
Fine paper	390	370	80	103	0.78
Liner	350	2300	140	214	0.64

5.3.4 Imaging the paper surface

Scanning electron microscopy, SEM, was employed in order to explore the paper surface properties of the two test paper types and the images are shown in Figure 5.2. The fibers in the fine paper showed a defined shape and the more flexible fibers in virgin pulp gave a more oriented fiber surface. The recycled fibers in the liner were more damaged and less flexible. It can also be seen that the liner contains more undefined material between the fibers. Also seen in Figure 5.2b) is the filler particles, calcium carbonate, as small, irregular, bright particles.
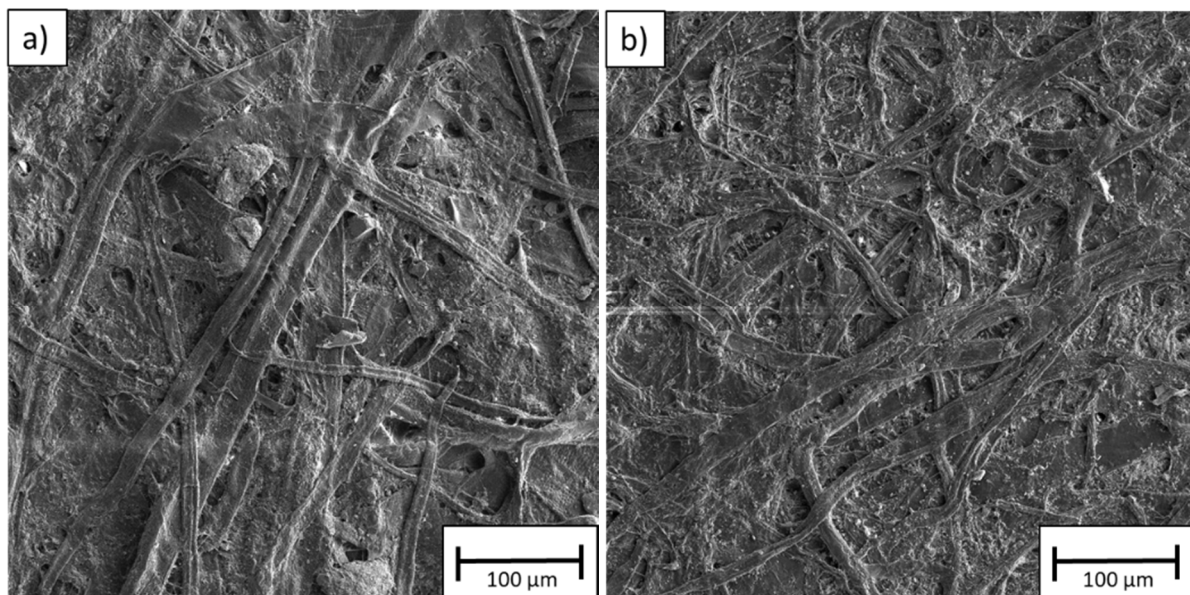

Figure 5.2. *SEM images of a) liner, b) fine paper.*

3D SEM images was obtained by analyzing 500 x 500 µm areas of the paper surfaces at different tilting angles (-10 ° and 10 °) and reconstructing the surface topography by combining the images. From the data analyses the specific surface area was obtained and presented as a ratio between specific area and projected area. The ratio for the fine paper and for the liner was 1.32 and 1.35, respectively, i.e. the specific surface area was similar for the two paper types. The difference in area ratio between the fine paper and the liner was lower than expected considering the difference in roughness obtained from the Bendtsen test. A rougher surface would be expected to have a larger specific surface area. However, the air flow measurements in the Bendtsen test are sensitive to variations in roughness and the overall specific surface areas that are determined from the 3D SEM images could still be similar. The discrepancy between the methods could also be due to difficulties related to the software to estimate the depth of the pores in the surface. In Figure 5.3 the reconstructed 3D images for fine paper and liner are shown. From these images, it is clearly seen that the fine paper has a smoother topography compared to the liner.
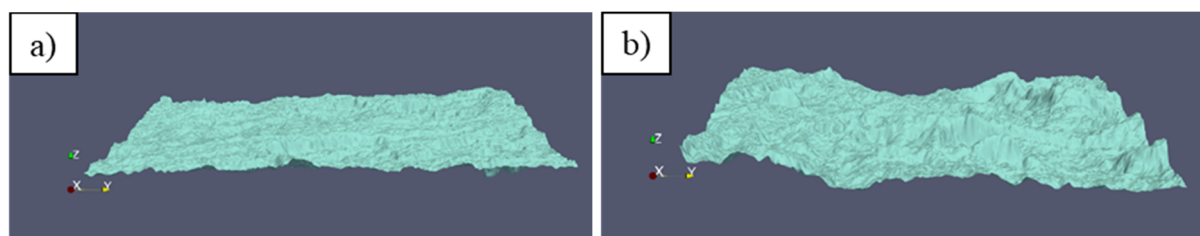

Figure 5.3. *3D reconstructed surface of a) fine paper and b) liner. The analyzed areas are 500 x 500 µm.*

The topography was evaluated further by fitting a plane to the surface and calculating the perpendicular distance from the plane for all the peaks and valleys on the surface. The height distributions from the plane are shown in Figure 5.4 demonstrating that the fine paper has a narrower, and shallower, height distribution compared to the liner.
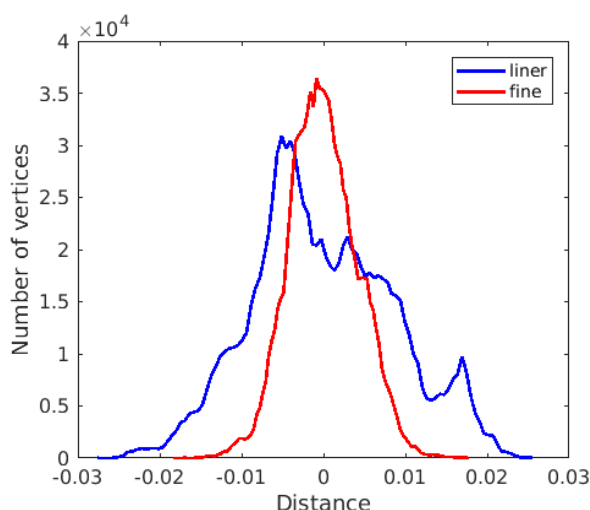

Figure 5.4. *Height distributions for liner and fine paper.*

TOF-SIMS of an untreated fine paper revealed the chemical composition of the surface and the imaging is shown in Figure 5.5. The fiber structure was clearly shown and the distribution of calcium carbonate and AKD can be seen. The internal sizing agent AKD

was included in the fine paper composition in order to prevent the hydrophilic paper from disintegrating during the surface sizing process.
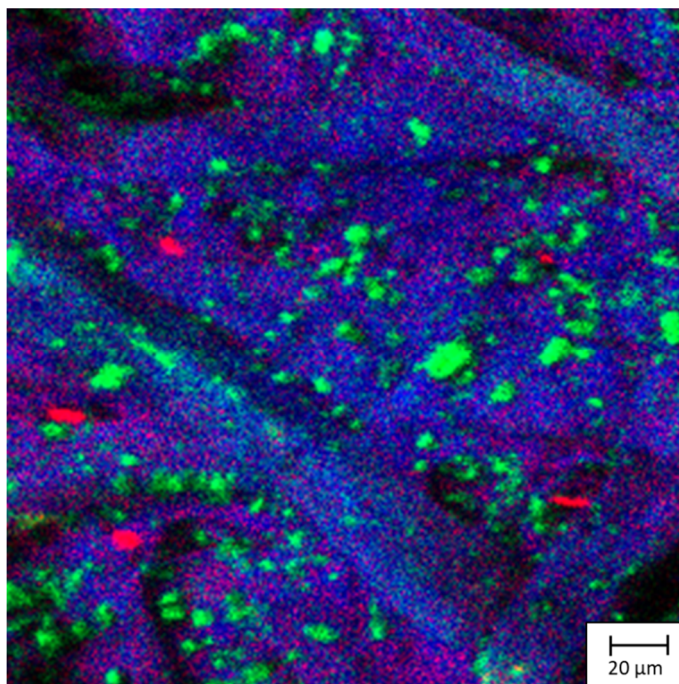

Figure 5.5. *TOF-SIMS imaging of the untreated fine paper surface. Calcium carbonate (green color) and AKD (red color) are clearly visible on the fiber structure (blue color).*

6   RESULTS AND DISCUSSION

6.1   THE COLLOIDAL SYSTEM

The particle types included in the studies described in this thesis have the same hydrophobic polymeric core, but different surface charge: strongly positive, weakly negative/positive or strongly negative. Despite having the same hydrophobic core, their ability to prevent wetting of a paper surface differs between the different particles. A comparison of the water uptake for SP+, SPA- and SP- is shown in Figure 6.1a, where a lower water uptake represents a more hydrophobic surface, which is the purpose of surface sizing. One can argue that the cationic particles have an advantage in having a charge opposite to that of the anionic fiber of which the paper surface is constituted, since then electrostatic attraction can take place. If the particles were applied solely on the paper surface this would have an impact, but in the regular case, and also in the study shown in Figure 6.1a, the particles are mixed with starch before being applied on the paper surface, as described in the Introduction. The source and the degradation method of the starch will influence its properties. Oxidized starch was used throughout the studies described here and since it is a polymer with anionic charges it can be regarded as a polyelectrolyte. Interaction of colloids with polyelectrolytes are described in the literature as having different origin depending on the charges. A colloid having a charge opposite to that of the polyelectrolyte can interact via electrostatic attractions[46-50] while a colloid bearing the same charge as the polyelectrolyte will encounter electrostatic repulsion and have attraction mainly by van der Waals forces.[29] The nanoparticles and the oxidized starch will thus have different modes of interaction depending on the surface charge of the nanoparticles, as illustrated in Figure 6.1b.
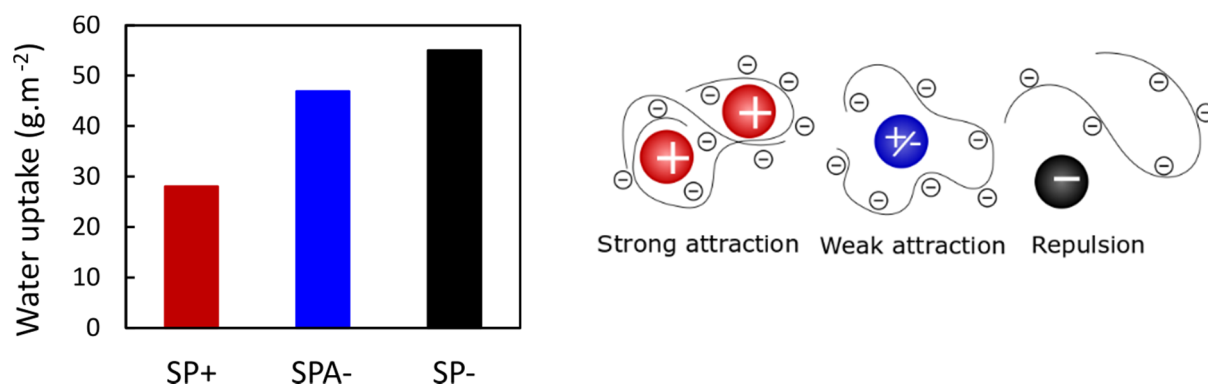

Figure 6.1 a) *Water uptake for test papers (liner grade) where the same amount of either SP+, SPA- or SP- was applied in combination with 8 wt. % oxidized starch.* **b)** *Scheme of possible interactions between the nanoparticles and the oxidized starch. Reprinted with permission from paper I ©2015 Elsevier.*

6.1.1 Effect of aggregation

The interactions between the particles and the oxidized starch was explored in a study of the colloidal behavior of the three particle types SP+, SP- and SPA-, as described in **Paper I**. It was observed that mixing oxidized starch with the cationic particles induced a loss of the colloidal stability of the system, seen as an increase in turbidity. With anionic and amphoteric particles, the colloidal stability was unaffected. Plots of turbidity versus starch concentration for the three particle types are shown in Figure 6.2.
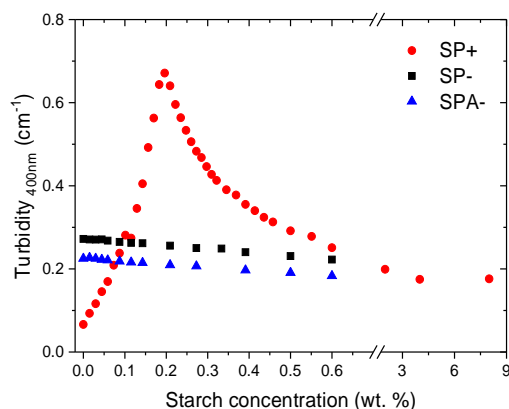
Figure 6.2. *Aggregation behavior for the different particle types. Reprinted with permission from paper I ©2015 Elsevier.*

The addition of starch to the SP+ particle suspension gave rise to an increase in turbidity due to formation of aggregates comprising the cationic particles and the anionic starch. The turbidity increase was seen already for the first aliquot, demonstrating that the colloidal stability was readily perturbed by the addition of an oppositely charged polyelectrolyte. The turbidity further increased with increasing starch concentration up to a maximum at a specific starch concentration. With further starch addition, above the maximum, the turbidity decreased but levelled out at an elevated turbidity compared to the non-aggregated system. This decrease in turbidity is attributed to a partial restabilization of the system while the higher value at the plateau compared to the initial value indicates that even with an excess of starch there are still aggregates present.

The system that gave the largest reduction in water uptake, displayed in Figure 6.1, was thus a system that underwent aggregation. In the study shown in Figure 6.1, the starch concentration was 8 wt. %, a concentration that is generally used in surface sizing. However, the maximum in turbidity occurred for the 0.1 wt. % SP+ suspension at a starch concentration as low as 0.2 wt. %, corresponding to a starch to particle mass ratio of 2:1. To correlate the aggregation behavior with the sizing performance, a surface sizing trial was performed using the liner grade as test paper, in which the efficiency in reducing the water uptake for the aggregating cationic and non-aggregating anionic particles was compared. The starch concentrations were 0.3 wt. % and 8 wt. %, which correspond to a starch to particle mass ratio of around 2:1 (corresponding to maximum aggregation) and around 50:1 (corresponding to the regular procedure), respectively.

Surface sizing results are shown in Figure 6.3. For the anionic particles, the degree of hydrophobization was unaffected by the starch concentration: the water uptake when

24

using 8 wt. % or 0.3 wt. % were similar. This is in line with the turbidity results that showed no interactions between SP- and starch. The cationic particles behaved differently and a superior degree of hydrophobization was seen when the starch to particle mass ratio corresponded to the higher aggregated state. The colloidal behavior can thus have a significant influence on the surface sizing performance.
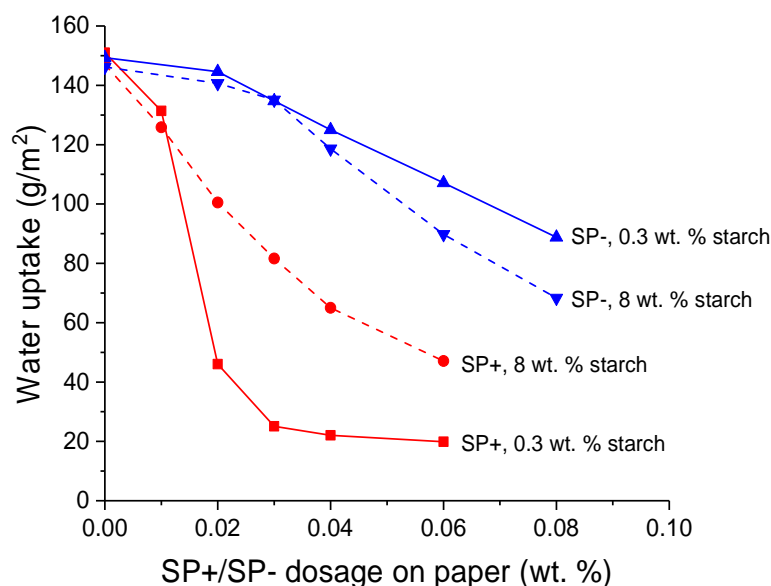

Figure 6.3. *Surface sizing results using either 0.3 or 8 wt. % starch together with either SP- or SP+. Reprinted with permission from paper IV ©2017 American Chemical Society.*

A plausible explanation can be that the formed aggregates are better retained on the paper surface due to attractive interactions with the starch. The entanglement of the starch chains give rise to an increased viscosity that will prevent deeper penetration and the cationic particles that are interacting with the starch will then benefit from this compared to the anionic particles that penetrate independent of the starch. The size of the formed aggregates is still small compared to the pore size of the liner grade so a filtering effect is not likely to occur.

6.1.2 Understanding the role of the aggregates
Aggregates formed by mixing SP+ and starch thus improve the surface sizing performance. Aggregate formation, composition, relaxation and stability have therefore been thoroughly investigated in this thesis work in order to understand how to control and take advantage of this aggregation behavior.

6.1.2.1 *Order of addition, mixing rate and particle concentration*
In studies of colloids and polyelectrolytes described in the literature it has been reported that the addition order, particle concentration and the mixing rate could influence the aggregate formation.[51-54] These parameters were evaluated for the system studied here and it was found that neither the addition order nor the mixing rate had an impact on the aggregates formed from SP+ and starch. The particle concentration had an impact on the magnitude of the turbidity, though. The turbidity increase was larger at higher

particle concentrations, however, the maximum in turbidity was always found at the specific starch to particle mass ratio of 2:1.

6.1.2.2 Maximum in aggregation at charge neutralization

The aggregation behavior of the cationic particles and starch was investigated further by DLS and by ζ potential measurements and the results are shown in Figure 6.4. The maximum in turbidity coincided with the maximum in aggregate size measured by DLS. The decrease in hydrodynamic radius for the aggregates beyond the maximum was however not as pronounced as the decrease in turbidity. One reason for this can be that the light scattering technique is very sensitive to size; the bigger the particles the larger is the scattering intensity. The ζ potential for the primary particles has the high positive value of +53 mV in Milli-Q water. When starch was added to the SP+ suspension, the oppositely charged polymer adsorbed on the particle surface due to electrostatic attraction and this induced a decrease of the ζ potential. At the maximum in turbidity and in size, the ζ potential crosses zero and the maximum in aggregation thus takes place at charge neutralization. With further starch addition, the ζ potential levels out on a slightly negative value, -8 mV. The formed aggregates were found to be stable for weeks, although the ζ potential was not sufficiently large for the system to regain electrostatic stabilization.[55, 56]
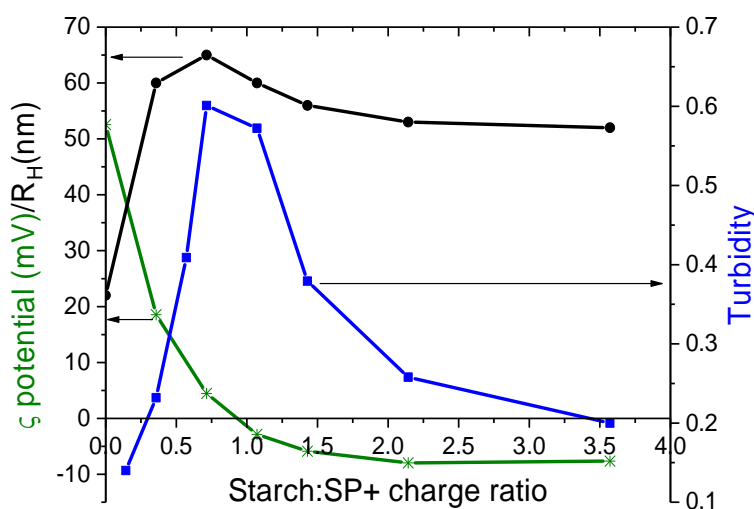

Figure 6.4. *Turbidity, hydrodynamic radius and ζ potential versus starch to SP+ charge ratio. The maximum in size corresponds to the point of charge neutralization. Reprinted with permission from paper II ©2016 Royal Society of Chemistry.*

6.1.2.3 Effect of starch composition – steric contribution

The oxidized potato starch that was used in this study consists of 80 wt. % amylopectin and 20 wt. % amylose.[37] Both polymers have the same repeating unit, glucose, but they differ in the degree of branching and in molecular weight. Amylopectin is a large, highly branched polymer while amylose is a relatively short, linear polymer.[37] In a SEC analysis the size distribution of the starch will therefore be bimodal where the peak corresponding to amylopectin will be eluted first and appear to the left in a

chromatogram. The chromatograms depicting the size distributions for the starch in solution before and after aggregate formation, are shown in Figure 6.5. From this figure, it can be seen that the composition of the starch solution was changed when aggregates had been formed. The peak corresponding to the larger, highly branched, amylopectin decreased to a larger extent in the supernatant compared to the peak corresponding to amylose. Thus, it seems that it was mainly the amylopectin fraction of the starch that participated in the aggregation with the cationic particles. This gives us a plausible explanation of the stabilization mechanism for the formed aggregates; the value of the ζ potential was too low for the system to have regained stability through electrostatic repulsion due to charge reversal. Instead the stabilization mechanism can be explained by electrosteric stabilization as a result of adsorption of the highly branched, high molecular weight amylopectin chains on the particle surfaces.
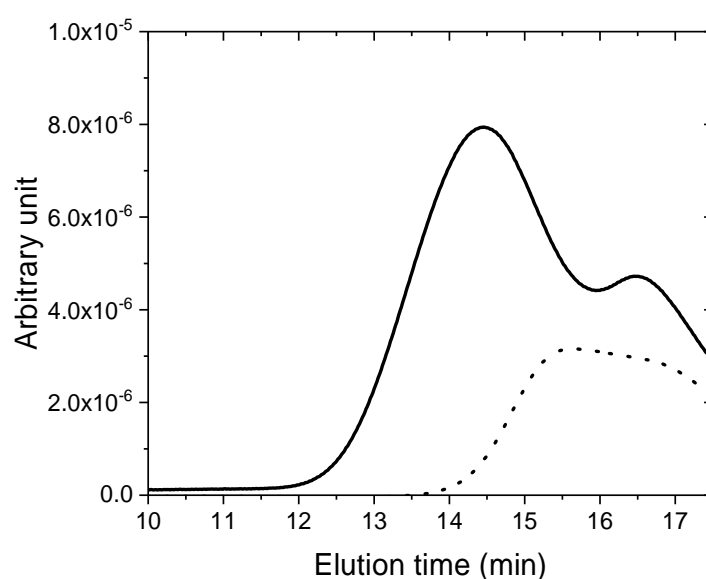

Figure 6.5. *SEC chromatograms of starch solution before (solid line) and after (dashed line) aggregate formation. Adapted from paper II ©2016 Royal Society of Chemistry.*

This steric contribution to the aggregate stabilization was also seen when the stability ratio of cationic particles and starch was evaluated. The stability ratio is defined as $W=k_{fast}/k$, where k_{fast} is the aggregate rate coefficient at maximum rate of aggregation and k is the aggregate rate coefficient in the studied conditions. The inverse stability ratio represents the likelihood of obtaining a dimer upon collision between two particles. For an electrostatically stabilized colloidal system, destabilization occurs when the electrostatic repulsions are screened and the hydrophobic interactions dominate. Screening of the particle surface charge was done by either addition of NaCl or addition of the oxidized starch. If only electrostatic repulsions had an impact, the stability ratio would approach 1, representing a completely destabilized system. This was true when NaCl had been added (900 mM). When starch was instead added, the stability ratio did not reach 1, confirming the hypothesis stated above that starch gives a steric contribution to the aggregate stability. In Figure 6.6 the stability ratio versus starch concentration for a model cationic particle type is displayed. The figure also shows the effect of variations of the electrolyte concentration.
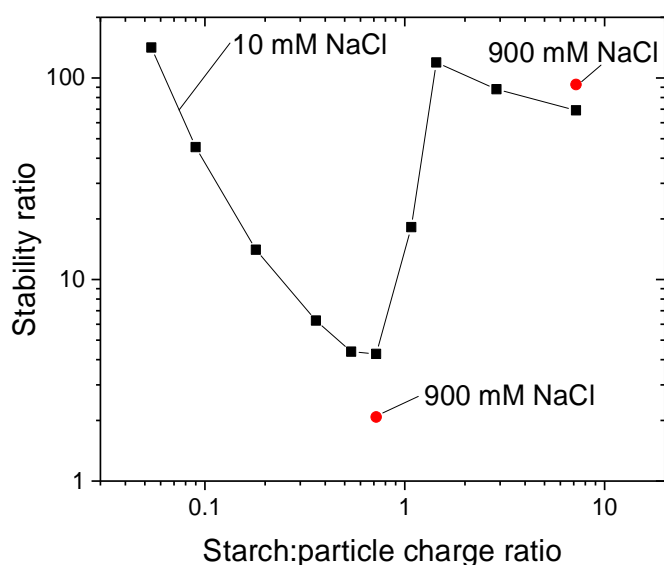
Figure 6.6. *Stability ratio, W, as a function of starch to particle charge ratio for amidine latex particles (AL110). 10 mM NaCl background was used (black squares). Two points with 900 mM background salt are also presented. Reprinted with permission from paper III ©2016 Royal Society of Chemistry.*

Aggregates formed at different starch to particle charge ratios were examined with small angle X-ray scattering (SAXS) in order to study the internal structures of the formed aggregates. The SAXS study showed that more and more starch was adsorbed onto the primary cationic particles up to charge neutralization. Starch adsorption above charge neutralization, which was seen as a charge reversal in the ζ potential measurements, was not seen in the evaluation of the SAXS data. Adsorption of anionic starch on a neutral or slightly anionic surface can occur due to the van der Waals forces. It is likely that starch adsorption above charge neutralization takes place primarily on the outer rims of the aggregates and the contribution to the surface coverage of the individual particles will thus be minor.

6.1.3 Mechanism of aggregation

In the literature, the aggregation of a charged particle and an oppositely charged polyelectrolyte is most often described as having a patchwise mechanism.[57-60] In the patchwise aggregation mechanism the polyelectrolyte chains are presumed to adsorb onto the particle surface due to electrostatic attraction. This leads to a local charge reversal on the particle surface, i.e. a patch of opposite charge is formed. This may lead to electrostatic attraction between covered patches on one particle and uncovered patches on another particle.[61] A mechanism via patchwise aggregation is proposed and described in Figure 6.7. When the anionic starch was added to the suspension of cationic particles, the starch, and mainly the amylopectin fraction of the starch, adsorbed on the particle surface due to electrostatic attraction. This adsorption is energetically favorable despite the loss of entropy that the starch experiences upon adsorption since the adsorbed polymer will replace many small counter ions and the net effect will be an entropy increase of the system.[29, 62, 63] The adsorbed starch will form a patch on the SP+ surface that can attract another cationic particle and eventually aggregates are formed.
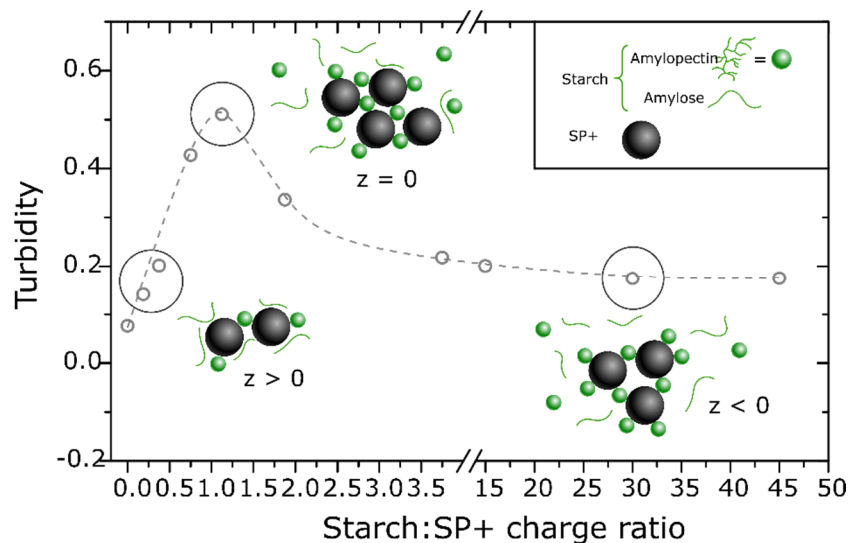
28

Figure 6.7. *Tentative mechanism for aggregation for regular starch, which is negatively charged and consists of a mixture of amylose and amylopectin, and SP+. Reprinted with permission from paper II ©2016 Royal Society of Chemistry.*

6.1.4 What happens if the starch type is changed to pure amylopectin?

As discussed above, SP+/starch aggregate formation was found to be beneficial for the surface sizing performance and it was concluded that it was mainly the amylopectin fraction of the starch that participated in the aggregation. It was therefore of interest to see if the aggregation, and thus the surface sizing performance, could be increased further by using a starch that consists only of amylopectin, a so-called waxy starch. In a surface sizing trial, the surface sizing performance of SP+ and SP- using waxy starch was compared. As with the regular starch, SP- was found to be unaffected by the starch concentration. SP+ was again found to have a further reduction in water uptake at the low starch concentration that corresponds to a maximum in aggregation, as seen in Figure 6.8, where water uptake versus SP+ dosage is shown when regular or waxy starch was employed. The water uptake results thus confirmed the hypothesis that a higher aggregated system will decrease the water uptake further. However, the difference between the high and low aggregated state was now minor compared to the results with regular starch where there was a reduction by 60 g/m^2 while for the waxy starch only by 30 g/m^2. It is likely that this is due to the magnitude of the aggregation. Turbidity and DLS data for the SP+/starch complexes formed with waxy starch (Figure 6.9) showed that larger aggregates were formed and that even at high starch to particle charge ratio the turbidity/size level remained high compared to when regular starch was employed. Thus, the "low" aggregated state for waxy starch was not so low.
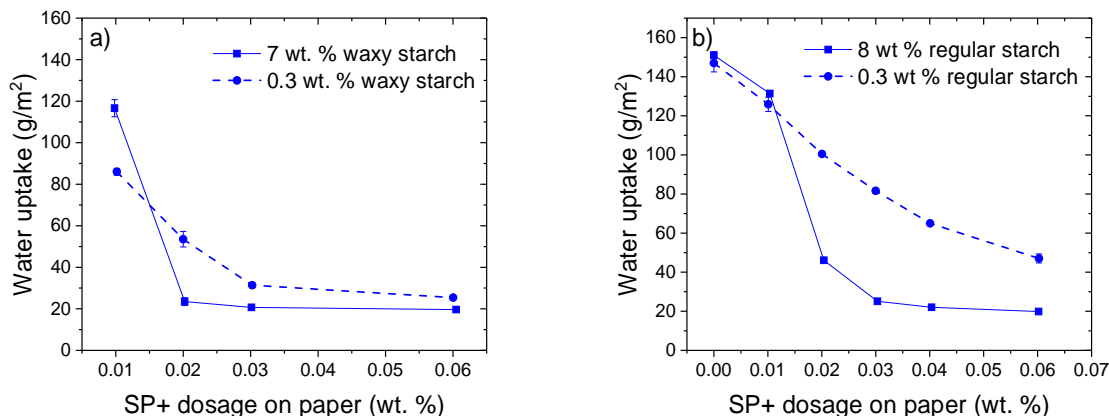
Figure 6.8. *Plot of water uptake versus particle dosage for SP+ with a) waxy starch or b) regular starch.*
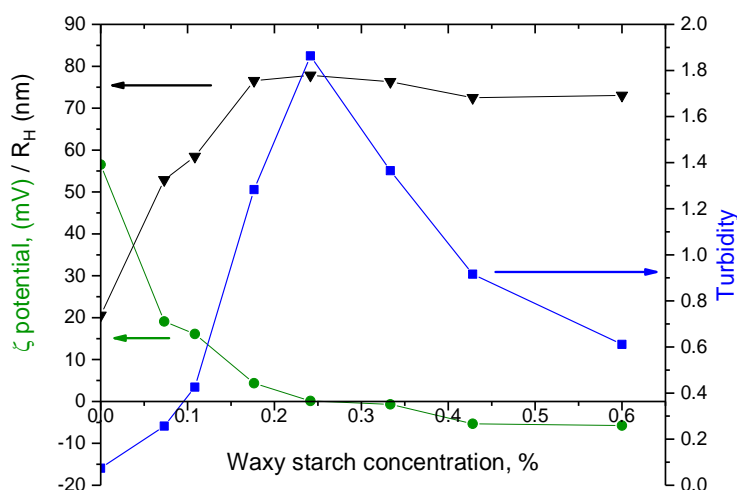

Figure 6.9. *Turbidity, hydrodynamic radius and ζ potential versus waxy starch concentration. The maximum in size corresponds to the point of charge neutralization.*

6.1.5 Non-equilibration flocculation - The kinetic effects

Aggregates formed by starch and SP+ are, as described in the previous chapter, important for the degree of hydrophobization. The understanding of the formation path and the stability of the formed aggregates are therefore of interest since this can create an opportunity to tailor the aggregates in order to enhance the surface sizing performance. The formation and relaxation of the aggregates were investigated in **Paper III**, in which the kinetic effects are also discussed.

When starch was added to the cationic particles the turbidity measured right after mixing was found to be higher than the equilibrated turbidity. This was attributed to an initial "non-equilibrium flocculation" (NEF).[64, 65] During NEF the time for particle collision, t_c, is shorter than the time for polymer relaxation, t_r. This could lead to a transition state and may result in an initial bridging flocculation.[66] With time, the starch chains will

30

relax into an equilibrated conformation, rendering starch patches on the particles and the aggregation mechanism will then evolve towards patchwise aggregation.[47, 67] Denser aggregates are subsequently formed, which leads to a decrease in turbidity with time. This is in agreement with the discussions in the literature about an initial aggregated state that with time will evolve into an equilibrated aggregated state.[64, 68-70]

The initial non-equilibrium bridging flocculation mechanism is supported by the turbidity results for SP+ in combination with waxy starch. A comparison between the two starch types with respect to initial and equilibrated turbidity is shown in Figure 6.10. The waxy starch gave rise to a larger difference between the initial and the equilibrated turbidity compared to the turbidity increase with the regular starch. The waxy starch contains only the highly branched, high molecular weight amylopectin and SEC analysis showed a higher Mw for the waxy starch compared to the regular starch. With a higher molecular weight, and thus longer polymer chains, bridging is promoted.[71]
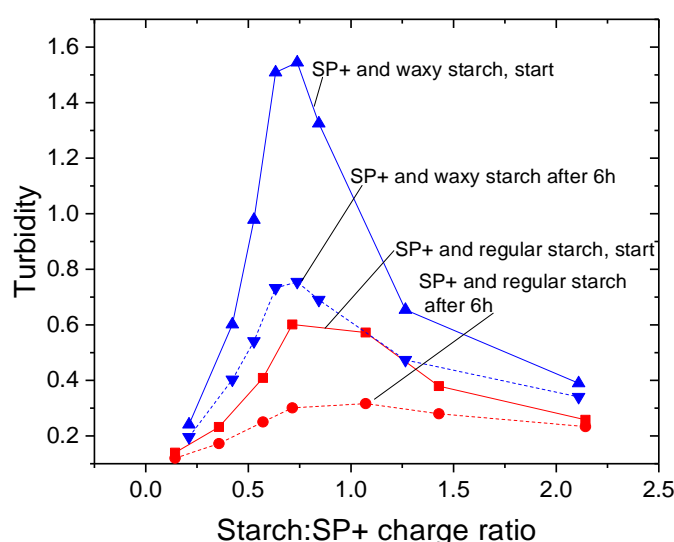

Figure 6.10. *Initial and equilibrated turbidity curves for SP+ with regular and waxy starch. The turbidity is measured as absorbance at 400 nm. Reprinted with permission from paper III ©2016 Royal Society of Chemistry.*

By monitoring the change of turbidity with time the kinetic pattern could be extracted; the turbidity value decreased with time until a plateau was achieved, i.e. when equilibrium was reached. Both the regular and the waxy starch in combination with the SP+ were monitored and it was found that the relaxation behavior was the same for both starch types. The relaxation behavior of the turbidity with time was evaluated by fitting the experimental data with the Kohlrausch-Williams-Watts (KWW) relaxation function. This function is used to describe various types of relaxation data and is often used as a universal model for studying various physical and chemical processes.[72-74] The evaluation of the kinetic data with KWW is described in detail in **Paper III**, where the main findings from the evaluation was that the relaxation time, τ, for the aggregates was the same irrespective of the position along the turbidity curve vs. starch concentration. In other words, irrespective of the particle to starch ratio and of the net charge of the

complex (as determined with ζ potential), the time for going from an initial aggregated state to the relaxed equilibrated state, where the starch chains have had sufficient time to rearrange on the particle surface, was the same. Interestingly, a difference between the starch types could be seen. This is shown Figure 6.11 where one turbidity curve for SP+ and regular starch and one turbidity curve for SP+ and waxy starch are plotted versus time together with the KWW fittings. On average, the relaxation time for the regular starch was around 1400 s and for the waxy starch around 4800 s. The waxy starch that has a higher molecular weight thus took much longer time for rearrangement of the polysaccharide chains on the particle surface. The higher anionic charge of the regular starch gives a stronger surface attraction.[75] This might also contribute to the difference in relaxation time between the regular and the waxy starch.
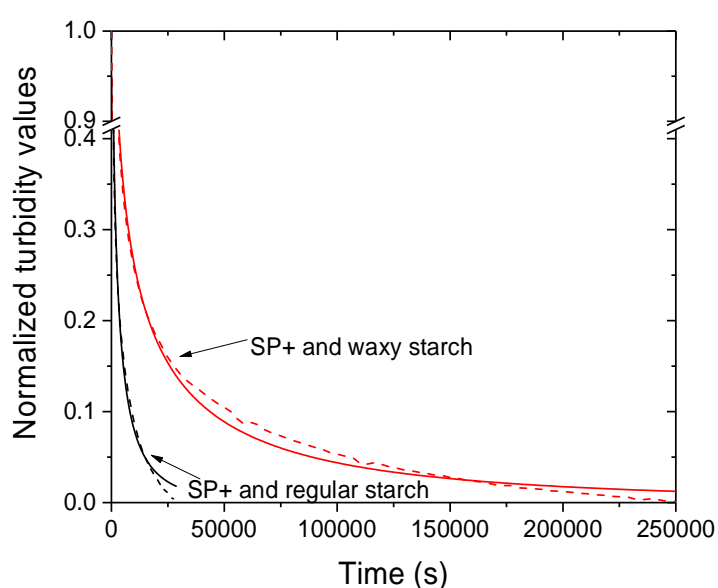

Figure 6.11 *Normalized turbidity data. For simplicity only one curve (dashed lines) for each starch type is shown in the figure together with the fitting of the KWW function (solid lines). Reprinted with permission from paper III ©2016 Royal Society of Chemistry.*

In the study of aggregate formation described in **Paper III**, larger cationic particles (AL110) where employed since the diffusion and thus the aggregate formation with SP+ and the regular starch was too fast to be captured with DLS. However, the findings that the kinetics with the waxy starch was slower prompted a DLS study with SP+ in combination with the waxy starch. It was possible to follow the aggregate *formation,* as well as the subsequent *relaxation,* for SP+ particles in combination with the waxy starch. The aggregate formation and the relaxation kinetics were monitored for the starch to particle charge ratio corresponding to maximum turbidity, i.e. close to neutrality. Figure 6.12 shows the results from these measurements with the size of the aggregates plotted against time. The aggregate *formation* gave rise to a rapid increase in size up to a plateau around 80 nm. With time, the size of the formed aggregates started to decrease due to relaxation of the starch chains. The aggregate size change levels out after approximately 500 minutes. This is in agreement with the turbidity measurements,

where it was found that the turbidity reached a plateau after a similar equilibration time. The increased size of the aggregates after long time compared to the primary particles showed that also after relaxation there were still aggregates in the system.
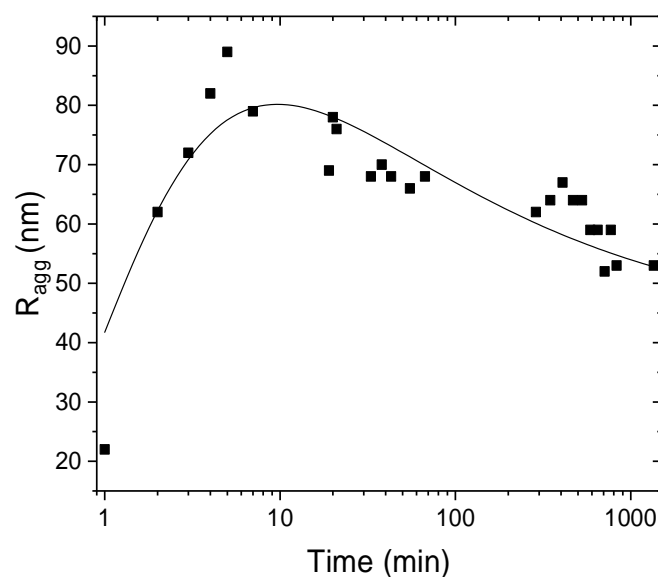

Figure 6.12. *Plot of radius of hydration versus time, demonstrating the aggregate formation and subsequent relaxation of SP+ in combination with waxy starch. Reprinted with permission from paper III ©2016 Royal Society of Chemistry.*

To study the effect of temperature, a series of experiments was performed at 40 °C and 60 °C and the results were compared to the turbidity results at room temperature. The overall colloidal behavior of the SP+ and starch combination was preserved at elevated temperature, i.e. the turbidity curves were similar and the maximum was at the same starch to particle charge ratio as at room temperature; however, the magnitude of the turbidity differed. There was a decrease in the turbidity at maximum with increasing temperature. When comparing the turbidity curve at 60 °C with the curve for the equilibrated values at room temperature a good agreement of the points was found. This is reasonable since the system is more dynamic at higher temperatures, which leads to a faster reorganization of the starch chains from bridging to patches on the particle surfaces.

These findings show that the relaxation rate after aggregate formation can be accelerated by an increased temperature or slowed down by an increased molecular weight of the starch; nevertheless, in the end the remaining, stable, aggregates will be the same. These results can be used to tune the state of aggregation by using either time, temperature or starch type as a controlling factor.

6.1.6 Influence of salt

In the proposed aggregation mechanism, the aggregation takes place due to electrostatic interactions. For a colloidal system stabilized by electrostatic repulsion, as in the case for the primary particles, or by electrosteric stabilization, as for the formed SP+/starch complexes, the interactions can be influenced by the ionic strength.[61] An increased ion

concentration in the bulk water will screen the electrostatic repulsions and may thus affect the colloidal stability of the system.[76] In a paper mill ions are always present. Originating from the hardness of incoming water, from additives at the wet-end or from recirculation of water the presence of ions may influence the surface sizing performance. The effect of increased ionic strength on the colloidal stability and the surface sizing performance was evaluated in **Paper IV**.

6.1.6.1 *Effect of salt on the colloidal stability of the particles*

An increased concentration of either NaCl, $CaCl_2$ or Na_2SO_4 was found to reduce the colloidal stability of the cationic particles while the anionic particles were unaffected. For SP-, the stabilizer is oxidized starch that is partly grafted into the particle core while for SP+ there is no evidence of grafting. This difference can explain why SP- is unaffected by an increased ionic strength. For SP- stability against flocculation is achieved by steric hindrance. For SP+, the screening of the surface charge allowed hydrophobic attractions to become more prominent. This can be seen visually by formation of large flocs that gave the particle suspensions a snowy appearance, as seen in Figure 6.13 where photographs of SP+ in salt solutions with an anion concentration of 20 mM are shown. Also, an effect of the valence of the anion can be seen; addition of Na_2SO_4 gave rise to larger flocs compared to when NaCl was added and the flocs started to form at lower salt concentration. No impact of the valence of the cation was seen when comparing NaCl and $CaCl_2$. This is expected since anions are known to have a stronger influence than cations on the stability of colloidal systems[77-79] and the valence of the anions is of particular importance. This is formulated in the modified Schulze-Hardy rule, which empirically correlates the ionic strength with the valence through $(1/z)^{4.9}$.[80] The actual value of the exponent for a specific system depends both on the surface charge density of the particles and on the nature of the co-ion of the added salt.[80]
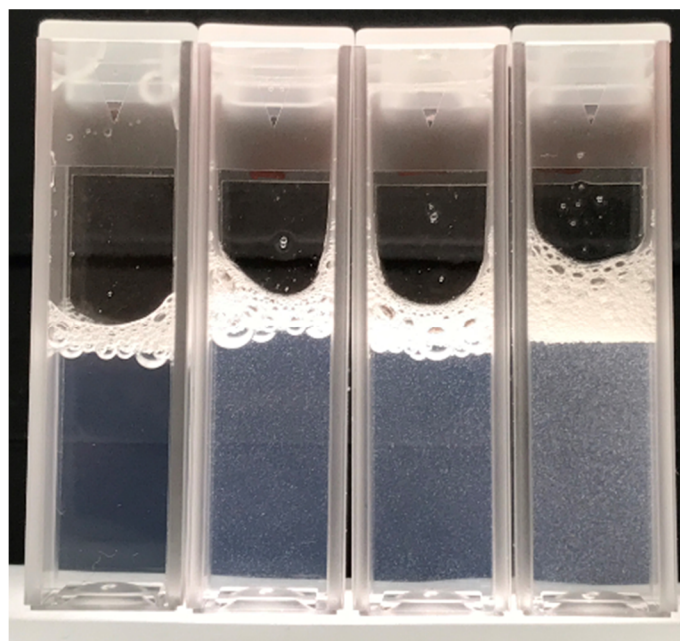

Figure 6.13. *An SP+ suspension, 0.1 wt. %, with the anion concentration of 20 mM. From left to right: reference without salt; with NaCl; with CaCl₂; with Na₂SO₄.*

When the size of the formed flocs was to be determined by laser diffraction a shear sensitivity of the flocs was discovered. In the laser diffraction instrument, a MasterSizer from Malvern, the sample is analyzed in a flow and the flow rate will induce shear forces. As a result, the flocs were broken. This was seen as a decrease in size with time as depicted in Figure 6.14.
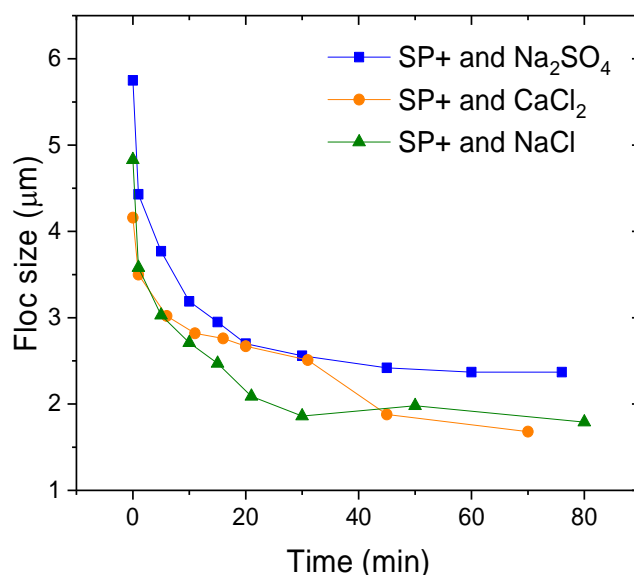

Figure 6.14. *Decrease in mean size with time monitored by laser diffraction measurements of SP+ and salts. The SP+ concentration was 0.4 wt. % and the ionic strength was 80 mM.*

6.1.6.2 Surface sizing at increased ionic strength

In the surface sizing procedure, the hydrophobic particles are most often combined with starch before being applied on the paper surface. However, the findings, discussed above, that SP+ forms flocs at elevated ionic strengths and that aggregate formation is beneficial for the reduction of water uptake of a surface sized paper, lead to a surface sizing trial where SP+ without starch was applied on the test papers, at different levels of ionic strength. Interestingly, depending on the salt type, the effect on the water uptake reduction was either positive, negative or neutral, as seen in Figure 6.15. When the ionic strength was increased with Na_2SO_4, SP+ formed the largest flocs and this resulted in an increase of the water uptake; thus, the addition of Na_2SO_4 was detrimental for the performance. Addition of NaCl did not significantly influence the water uptake results, even though also NaCl induced floc formation for SP+ at the ionic strengths used in the trial. This may be attributed to the shear sensitivity of the formed flocs. In the size press the particle suspension is pumped through the equipment and this might cause sufficient shear to destroy the flocs formed when the ionic strength was increased by NaCl. Addition of $CaCl_2$ gave rise to a further decrease in water uptake, which was unexpected. One may speculate that this effect is due to specific interactions of calcium ions with carboxyl groups on the paper surface.[81, 82]
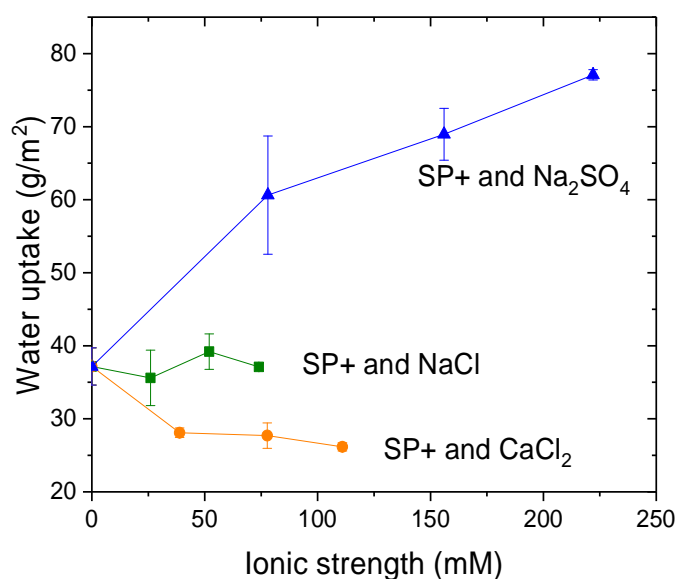
Figure 6.15. *Plots of water uptake versus ionic strength for NaCl, CaCl₂ and Na₂SO₄. Reprinted with permission from paper IV ©2017 American Chemical Society.*

6.1.6.3 Salt effect on the SP+/starch complexes

An increase in the ionic strength was also found to influence the formed starch/SP+ complexes and the effect was depending on the starch to SP+ charge ratio, ionic strength and time. It was found that upon salt addition, the turbidity initially decreased in a similar manner irrespective of the starch to particle charge ratio, with the exception of the lowest ratios. This was attributed to a "screening-reduced adsorption" that occurs when the attraction between the polymer and the particles is mainly of electrostatic nature.[83] In parallel the salt also had an impact on the starch. At low ionic strength the polyelectrolyte is stretched out to maximize the entropy gain for the counter ions. When the ionic strength is increased, the entropy gain decreases[29], which causes contraction of the starch chain.[76, 83, 84] This leads to a more coiled structure that gives a denser packing on the particle surface, i.e. the starch behaves like an uncharged polymer where loops and tails are formed.[85-87] The increase in turbidity at increased ionic strength is thus most likely due to additional bridging[86, 88] and this effect is described in the literature as "screening-enhanced adsorption".[83] This time dependent turbidity is displayed in Figure 6.16.
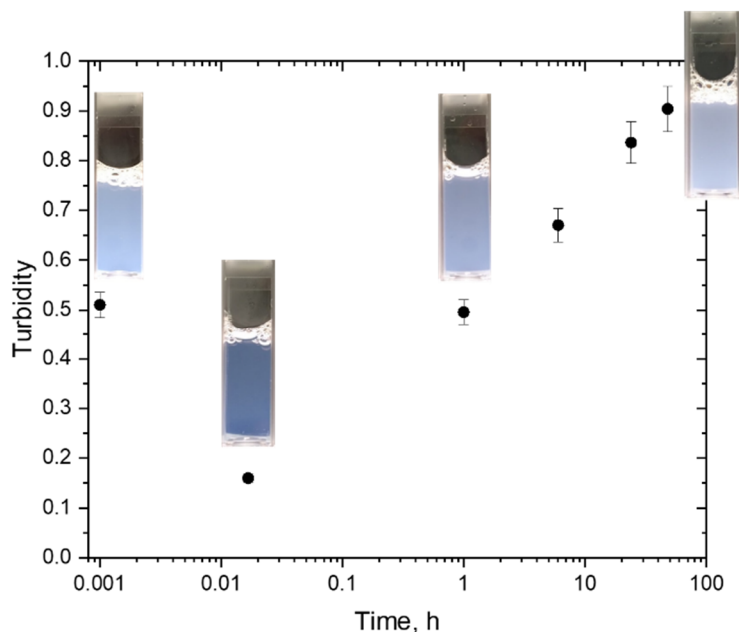
Figure 6.16. *Evolution of turbidity with time for SP+/starch complexes at a starch to SP+ charge ratio of 0.7:1 in presence of 26 mM NaCl. Reprinted with permission from paper IV ©2017 American Chemical Society.*

After approximately 48 hours the turbidity had reached a stable value and the system was then regarded as equilibrated. The turbidity results for the different starch to SP+ charge ratios as a function of ionic strength (NaCl) are shown in Figure 6.17. The higher the starch to SP+ charge ratio, the lower was the maximum in turbidity. At higher ratios more starch is adsorbed on the particle surface, contributing to steric stabilization and thus preventing aggregate growth. The maximum in turbidity was also shifted towards higher ionic strength for the higher starch to SP+ charge ratios. The adsorbed starch thus seems to have an inhibiting effect on the aggregate formation in the presence of salts. The order of addition was found not to influence the formed complexes of SP+/starch/NaCl. The same turbidity effect was achieved when NaCl was added to a SP+/starch mixture as when starch was added to a SP+/NaCl mixture.

Using CaCl$_2$ instead of NaCl to increase the ionic strength gave rise to a similar effect on turbidity, which could thus be correlated to the chloride ion concentration. Hence, the aggregation at elevated ionic strength increased by either NaCl or CaCl$_2$ is due to a specific anion effect and not to the ionic strength *per se*. When Na$_2$SO$_4$ was added in similar ionic strength ranges as NaCl or CaCl$_2$, no increased turbidity was seen, instead flocs were formed already at the lowest ionic strength used, demonstrating the stronger effect from the divalent anion.
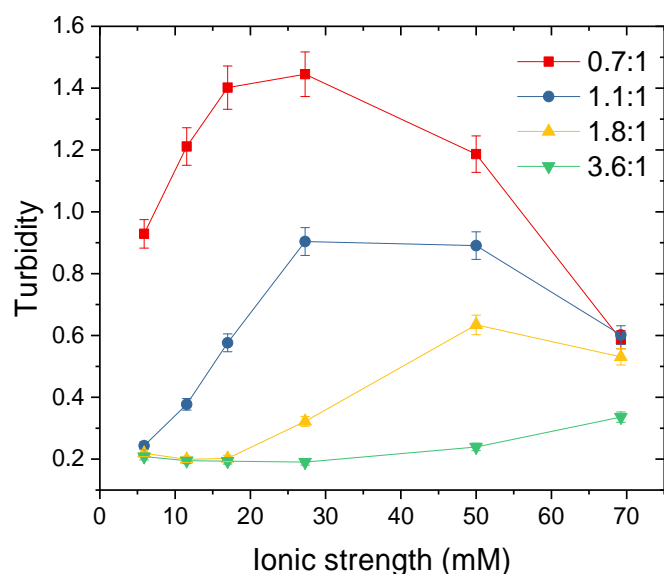
Figure 6.17. *Impact of starch to SP+ charge ratio (from 0.7:1 to 3.6:1) on the turbidity with increasing ionic strength. Reprinted with permission from paper IV ©2017 American Chemical Society.*

The size distributions for the SP+/starch complexes with a charge ratio of 0.7:1 at the NaCl concentration corresponding to maximum in turbidity were evaluated by dynamic light scattering. A bimodal distribution was found for the SP+/starch/NaCl complexes, clearly different from the monomodal distribution seen for SP+ and the SP+/starch complexes. A comparison of the size distributions is shown in Figure 6.18.
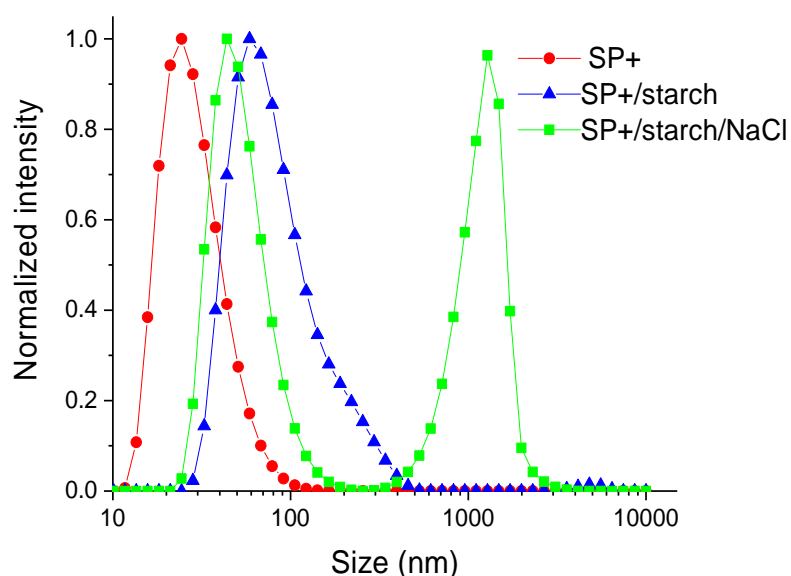
Figure 6.18. *Normalized volume average size distributions for SP+, for the SP+/starch complex and for the aggregate formed by SP+/starch at an ionic strength of 26 mM NaCl. Reprinted with permission from paper IV ©2017 American Chemical Society.*

A closer examination of the turbidity curves in Figure 6.17 reveals a decrease in the measured turbidity for the two charge ratios 0.7:1 and 1.1:1 at the highest ionic strengths used in the study. This is an apparent decrease due to sedimentation of the larger flocs that are present also at lower ionic strength, as indicated by the size distributions in Figure 6.18. At the highest ionic strengths these flocs are dominant and will settle with time, which leads to lower turbidity values.

6.1.6.4 *Surface sizing at increased ionic strength with starch present*

Aggregate formation in presence of a salt has a different mechanism compared to when SP+ was combined with starch in Milli-Q water; the rate of formation was slower and the size distribution was bimodal. When the influence of salt on the surface sizing performance with starch present was evaluated, the SP+/starch/salt mixture was therefore let to equilibrate before application. Surface sizing trials were performed in which SP+ was mixed with starch and the ionic strength subsequently increased by addition of either NaCl, $CaCl_2$ or Na_2SO_4. The starch concentration used was 0.3 wt. %, corresponding to the starch to SP+ ratio that gives maximum surface sizing effect. The results from the surface sizing trials with increased ionic strength are shown in Figure 6.19. From this figure it can be seen that the addition of salts to the SP+/starch mixture was detrimental for the performance since the water uptake increased with an increase in salt concentration. Thus, the ionic interaction with the SP+/starch complex that gave an increased turbidity influenced the surface sizing performance in a negative manner.

The results from the colloidal studies were found to correlate with the surface sizing performance at elevated ionic strength. Figure 6.19a shows the water uptake as a function of chloride ion concentration and the influence on the SP+/starch complexes by NaCl or $CaCl_2$ was found to be very similar, demonstrating the anion effect and that the influence from the cation was negligible. The effect of the valence is also evident, as shown in Figure 6.19b. The larger effect of Na_2SO_4 than of NaCl is seen as a steeper increase in water uptake when the ionic strength is increased.
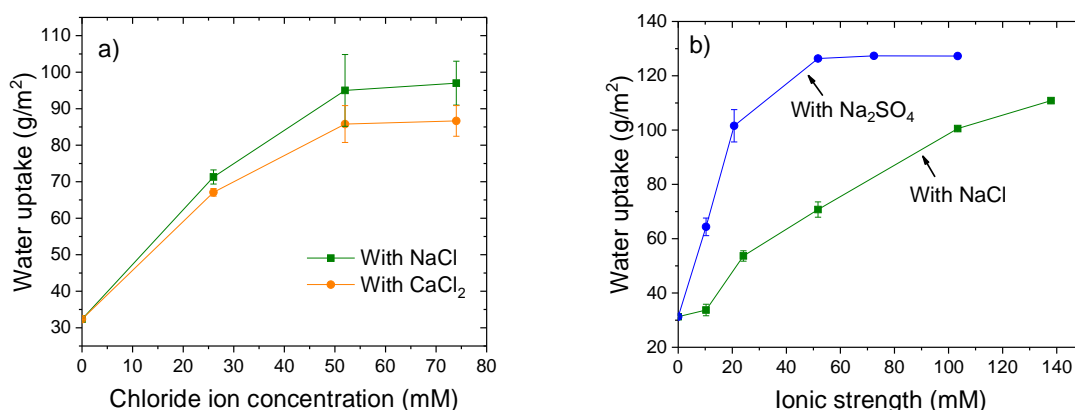

Figure 6.19 a) *Water uptake for SP+/starch when NaCl or $CaCl_2$ was added, plotted versus chloride ion concentration. b) Water uptake for SP+/starch when NaCl or Na_2SO_4 was added, plotted versus ionic strength. Reprinted with permission from paper IV ©2017 American Chemical Society.*

The plots of turbidity versus ionic strength for the different charge ratios (Figure 6.17) showed a decrease in the turbidity maximum with increasing amount of adsorbed starch, which was interpreted as prevention of aggregate growth due to steric hindrance by the starch. This effect was also seen when the starch concentration was increased from 0.3 wt. % to 8 wt. %. The results from the surface sizing trial are shown in Figure 6.20, where the impact of both NaCl and Na_2SO_4 was found to be much less pronounced when 8 wt. % starch was used.
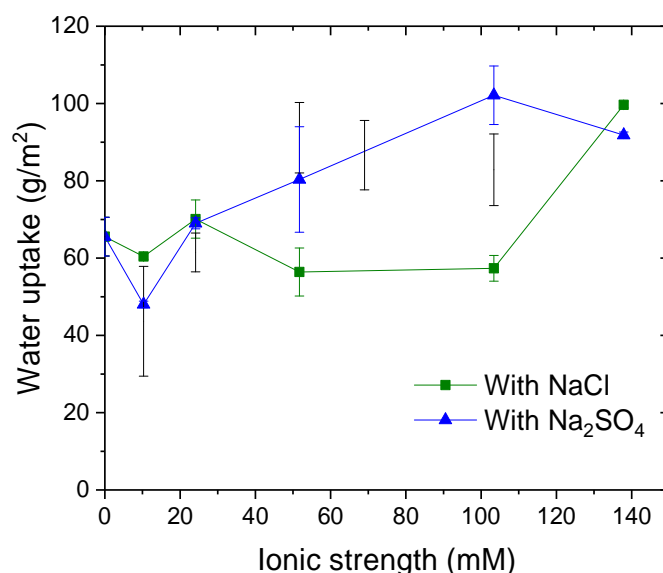
Figure 6.20. *Water uptake for a surface sizing trial with SP+ when 8 wt. % starch was used and with NaCl or Na_2SO_4 added as electrolyte. Reprinted with permission from paper IV ©2017 American Chemical Society.*

The influence of salt on the SP+/starch complexes and the effect on surface sizing performance shows that aggregation is not always beneficial. An optimized aggregation can boost the performance but it is not as simple as "the bigger the better". The large aggregates/flocs that were found to form in the presence of salts were detrimental for the surface hydrophobization effect.

The studies of the salt effect were mainly focused on SP+ since it was SP+ that formed aggregates due to electrostatic interactions with the oxidized starch. In some studies SP- was included as a reference system that does not form aggregates; however, the results showed that SP- exhibited a different, and interesting, behavior at increased ionic strengths. First, as stated above, the hydrophobic interactions between the cationic particles that caused floc formation did not take place for SP- in the presence of either NaCl, $CaCl_2$ or Na_2SO_4. This was attributed to steric hindrance from the stabilizer that in the case of SP- was starch. Since SP- does not form flocs, the surface sizing performance could be assumed to be unaffected by an increase in ionic strength; however, this was not the case. It was found that when SP- was employed in combination with 0.3 wt. % starch at an increased ionic strength, the water uptake decreased with increasing ionic strength, as displayed in Figure 6.21. In this figure the effect of NaCl and $CaCl_2$ is shown, and the same trend was also found for Na_2SO_4. The reason for an

enhanced water uptake reduction at elevated ionic strength may be a screening effect. The anionic charges of SP- are effectively screened by the salt addition, causing better retention of SP- on the anionic cellulosic fibers at increased ionic strength.
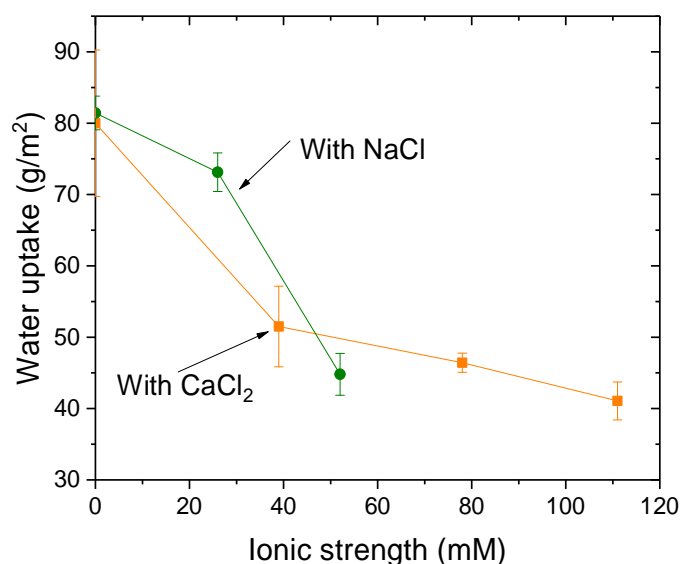

Figure 6.21. *Plot of water uptake versus ionic strength for SP- and 0.3 wt. % starch, in the presence of NaCl or CaCl₂.*

6.1.7 Composition or charge?

In most of this thesis work SP+ and SP- have been investigated and compared. However, the two particle types differ both by size (50 nm for SP+, 72 nm for SP-), surface charge and stabilizer type. While SP+ has a synthetic polymer as stabilizer, SP- is stabilized with degraded, oxidized starch. To determine whether the colloidal behavior and superior surface sizing efficiency encountered for SP+ is a specific feature for this type of hydrophobic nanoparticle or if it is a generic effect for cationic particles, the starch-based, net cationic particle type, SPA+, was included in a series of experiments. The colloidal stability was found to be affected for SPA+ in the same manner as for SP+. A turbidity increase was seen for the first aliquot added to the SPA+ suspension and the turbidity maximum was found at a lower starch to particle mass ratio compared to SP+, due to the lower surface charge for SPA+. A subsequent restabilization of the system with starch addition passing the maximum in turbidity was seen as a decrease in turbidity until a plateau was reached. A surface sizing trial was performed where SP+, SPA+ and SP- were compared. The trial was done with 8 wt. % starch, both on the liner and the fine paper. Figure 6.22 shows the results from the trial. The reduction in water uptake for SPA+ is larger than for SP- and the only difference between those two particle types is the (net) surface charge. SP+ is performing better than SPA+, thus it seems that a positive charge is important and the stronger the charge, the better.
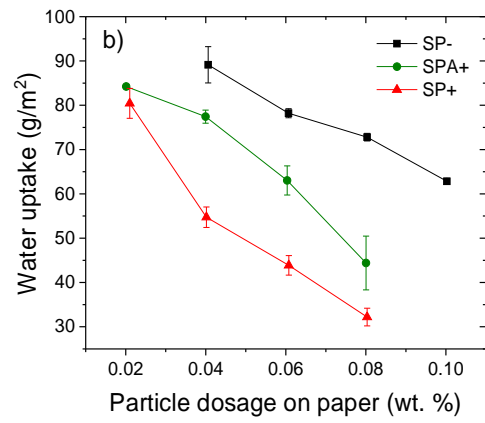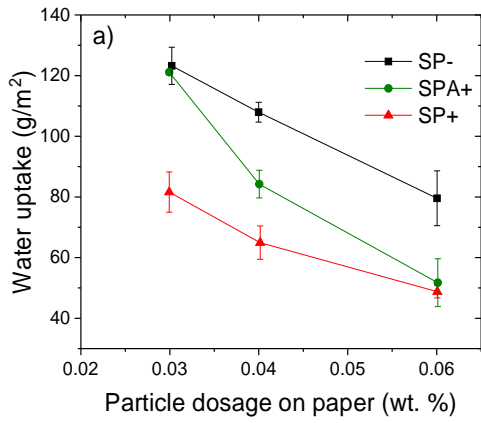
Figure 6.22. *Plots of water uptake versus particle dosage for SP+, SP- and SPA+. a) Applied on a liner grade, b) applied on a fine paper grade.*

6.2 THE SURFACE

6.2.1 Surface structure

The properties of the test papers that were employed in the surface sizing trials are described in Chapter 5.3. From the characterization it can be concluded that a paper surface is rough, porous and heterogeneous. The roughness and porosity originate from the fiber structure that is the main constituent of a paper and the heterogeneity is due to additives and wood residues like lignin and fatty acids. Surface sizing starch is applied on the paper surface in order to increase the surface strength[14] and to smoothen the surface while the nanoparticles are applied to add hydrophobicity to the paper surface.

SEM pictures were taken of both untreated and surface sized paper to examine the impact of the surface sizing on the structure of the paper surface. Both fine paper and liner were examined. In the pictures shown in Figure 6.22 a-d it can be seen that addition of starch leads to a somewhat denser surface structure for both paper types. For the paper sheets that were surface sized with SP+, SPA- and SP- no further densification could be seen and no other signs of the presence of the surface sizing particles could be established with this method (results not shown).
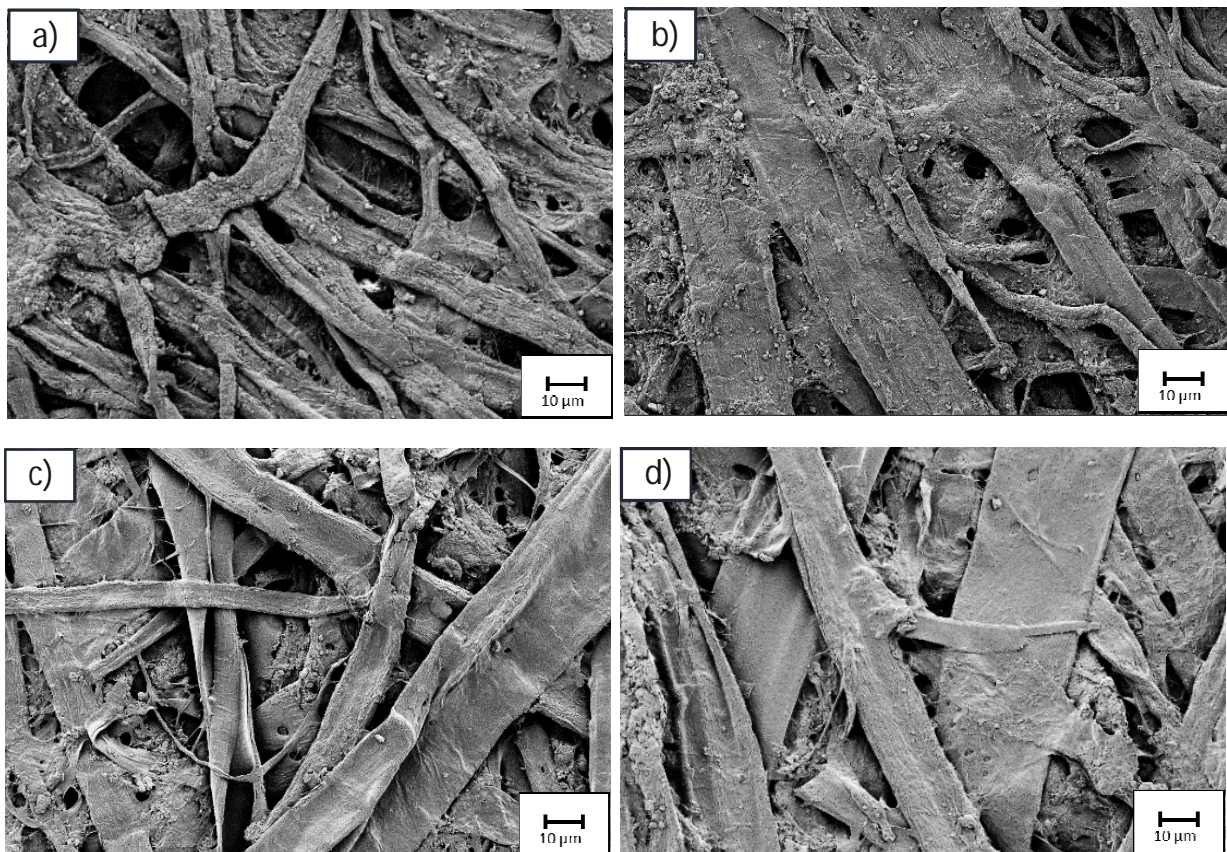

Figure 6.22. *SEM images of a) unsized fine paper, b) fine paper sized with starch, c) unsized liner, and d) liner sized with starch.*

When starch was applied on the paper surface, the air permeability for both the liner grade and the fine paper grade decreased. The starch film will fill the surface voids in the paper sheet and thus reduce the porosity.[12] No additional decrease in air permeability could be seen for neither the fine paper grade nor the liner grade when the mixture of starch and particles was applied. This is in line with the findings in previous studies of surface topography on similar systems, where it was concluded that surface sizing particles do not affect the surface structure.[89] The roughness of the fine paper grade was not affected by the starch application since untreated fine paper sheets already have a smooth surface due to the high filler content.[4] On the other hand, the roughness of the liner was significantly decreased by the starch application, which is according to expectations since unsized liner has a high surface roughness compared to fine paper. However, no further increase in smoothness could be seen upon addition of the particles.

6.2.2   Water retention

The untreated fine paper grade had a water uptake value of 81 g/m^2. After exposure to starch at a concentration of 8 wt. %, the water uptake increased to 107 g/m^2, which is an indication of a more hydrophilic paper surface, also observed in previous studies.[6, 89] The same effect was seen for the liner, for which the untreated paper had a water uptake of 137 g/m^2, a value that on exposure to starch increased to 154 g/m^2. Figure 6.23 shows the results from surface sizing trials for SP+ and SP- on the two paper grades, using an increasing concentration of sizing particles while the starch concentration was kept constant at 8 wt. %. From these trials it can be concluded that SP+ has a superior performance compared to SP-, both on the liner and on the fine paper. For SP-, the impact of dosage was less pronounced for the fine paper than for the liner, as seen in Figure 6.23 by the smaller slope. This means that higher amounts of SP- are needed when applied on the fine paper compared to when applied on the liner in order to reduce the water uptake to the same extent. However, for SP+, the shape of the curve was the same irrespective of whether the fine paper or the liner grade was used. Thus, the paper type seems to influence the surface sizing performance more for SP- than for SP+.
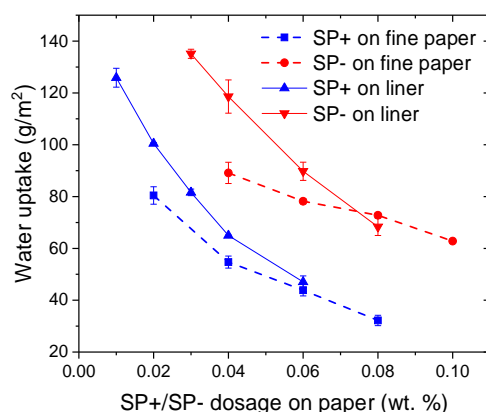

Figure 6.23. *Water uptake versus particle dosage for SP+ and SP- in combination with 8 wt. % starch when applied on either liner or fine paper. Note; this figure is a merger of several trials (SP+/SP- on fine paper/liner were tested separately) and the interpretation should therefore only be on trends, not on absolute values.*

6.2.3 Influence of starch concentration

In the surface sizing procedure, starch is most often added in order to increase the surface strength of the paper[14] and in some cases also for smoothening the surface. A starch concentration of 8 wt. % was used as a standard concentration in the surface sizing method used here and was in accordance with starch concentrations used in other related studies.[90, 91] However, as discussed above, starch was also found to have an active role in the formation of aggregates when SP+ was used as hydrophobic nanoparticles and this was found to be beneficial for the surface sizing performance, especially at a lower starch concentration that corresponded to a 1:1 charge ratio.

From a surface hydrophobization perspective, starch will counteract the effect from the hydrophobic nanoparticles since it is intrinsically hydrophilic. On the other hand, a smoother, less porous surface will have a lower water uptake rate. The two contradictory effects of starch were evaluated by using different starch concentrations in surface sizing trials that were performed on the liner grade using either SP+ or SP- in combination with different starch concentrations: 0, 2, 4 and 8 wt. %. The starch concentration will affect the solution viscosity and thus influence the wet pick-up.[14] The variations in wet pick-up were taken into account and the SP+/SP- dosage was adjusted accordingly. At starch concentrations of 2, 4 and 8 wt. %, the SP+/starch aggregation had reached a plateau value and the formed aggregates were thus not significantly affected by the difference in starch concentration. For SP- the starch concentration did not have an impact on the colloidal behavior, which means that the performance of SP- should be independent of the starch concentration.

The results from the surface sizing trials for SP+ and SP- combined with the different starch concentrations are shown in Figure 6.24. For all starch concentrations, SP+ has a superior performance compared to SP-. This was expected since the aggregation of SP+ with starch has in previous studies been found to be beneficial and in the starch concentrations range used in this study, SP+/starch complexes are present. When no starch was used in the surface sizing trial, the cationic particles will, as a result of electrostatic attraction, be retained on the paper surface and thus still give better performance compared to SP- that carries the same charge as the fibers in the test paper.
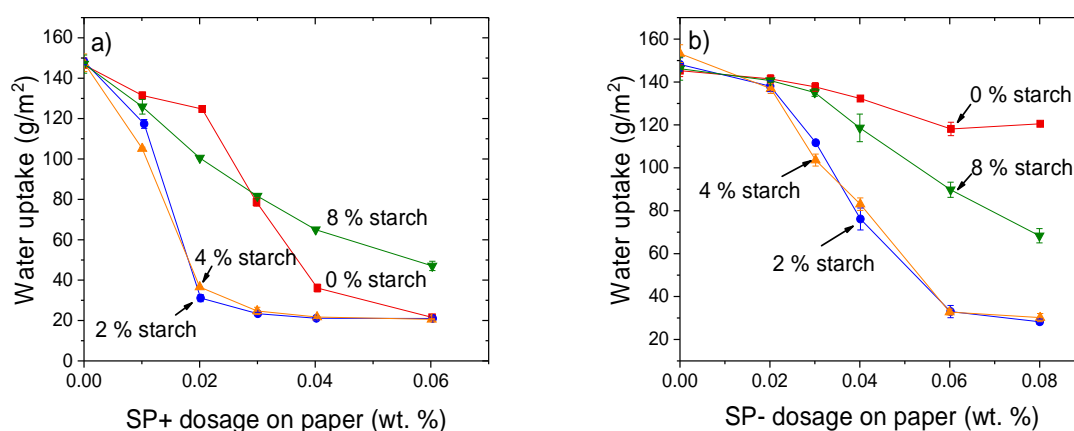

Figure 6.24. *Water uptake plotted versus dosage of a) SP+ and b) SP-, in combination with 0, 2, 4 and 8 wt. % starch.*

An interesting and somewhat surprising result was the reduction in water uptake for both SP+ and SP- at intermediate starch concentrations: 2 and 4 wt. % starch. The water uptake curves for both SP+ and SP- at these starch concentrations had a much steeper slope compared to when 8 wt. % starch was used, as seen in Figure 6.24. The impact of the starch concentration thus seemed to be a general effect. A tentative explanation could be that application of starch on the paper surface has an optimum somewhere. Too low an amount of starch on the paper surface is not sufficient to decrease the porosity and thereby decrease the rate of water uptake and too high an amount on the surface will increase the hydrophilicity of the paper, thereby counteracting the desired hydrophobization effect achieved with the hydrophobic nanoparticles SP+ and SP-.

6.2.4 Distribution of positively charged nanoparticles on and in the paper sheet

A central question in this thesis work has been how the nanoparticles can be so efficient in reducing the water uptake. Calculations show that the amount of nanoparticles added to achieve good effect is not enough for forming a monolayer on the porous paper surface. Time of flight secondary ion mass spectroscopy, TOF-SIMS, is a technique for chemical characterization of a surface with high spatial resolution. This technique was employed to investigate the distribution of SP+ on the paper surface and in a cross-section of the paper sheet. The aim of the study was to explore the importance of the surface and the cross-sectional distribution of the nanoparticles on the hydrophobization. The results presented here are new, unpublished data that will be included in a future publication.[92]

6.2.4.1 Surface distribution

Images from the TOF-SIMS characterization of the surface sized fine paper sheets are shown in Figure 6.25. In this figure the surface distribution of the cationic particles is displayed for the lowest and the highest SP+ dosages used in the trial. The SP+ distribution is shown in red while the internal sizing agent, AKD, is in green and the fibers are in blue. AKD was added to the pulp in order to prevent the hydrophilic fine paper to disintegrate during the surface sizing procedure. It is clear from the image that a higher dosage of SP+ in the size press leads to a higher surface coverage.
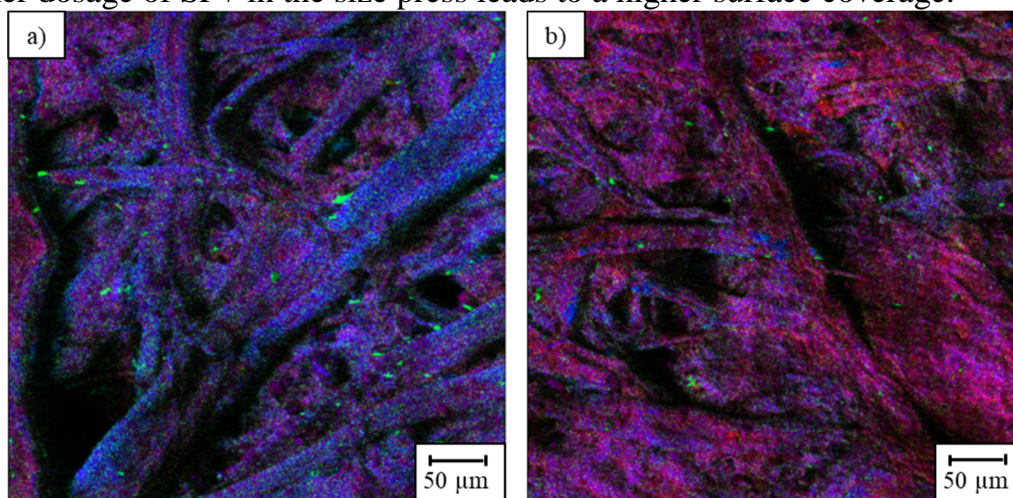

Figure 6.25. *TOF-SIMS images for a) low dosage and b) high dosage of SP+. The SP+ distribution is displayed in red color, the AKD distribution in green color and the cellulosic fibers are displayed in blue color.*

To quantify the amount of each component on the surface, a model that was based on the reference spectrum of each component was used. A mean pixel percentage could be obtained by utilizing classical least squares fitting of the reference spectra to the spectra at each pixel. (The pixels in the final image are binned pixels, 2x2, to increase the signal strength.) The mean pixel percentage for the four components present on the paper surfaces treated with starch in combination with low, medium or high dosage of SP+, are summarized in Table 6.1. The surface coverage of SP+ increases from the low to the medium dosage but no significant difference is seen between medium and high SP+ dosage. Assessment of water uptake reduction by the Cobb60 method showed a linear decrease in water uptake for the three SP+ dosages; thus, there is a discrepancy between the Cobb60 results and the TOF-SIMS results. When instead comparing the values obtained with TOF-SIMS with contact angle measurements for the three SP+ dosages, a correlation can be seen. The contact angle values measured by the sessile drop method for the three SP+ dosages correlate with the mean pixel values for SP+. The drop that is applied on the paper surface during the contact angle measurement rests on the surface and is small enough not to be pressed into the paper due to gravity. The contact angle is thus solely governed by the hydrophobicity of the outermost layer of the paper sheet, i.e. the surface, and that is also what is captured with TOF-SIMS. The results from the sessile drop measurements are shown in Figure 6.26.

Table 6.1. *Mean pixel percentage for the components found in papers treated with starch only, as well as starch in combination with low, medium or high dosage of SP+.*

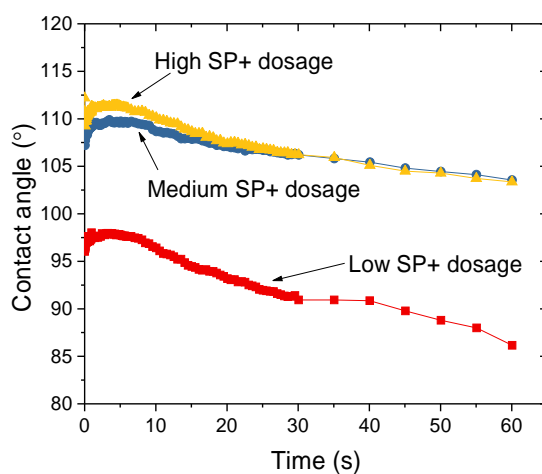| Component	Starch only	Low SP+ dosage	Medium SP+ dosage	High SP+ dosage
SP+	-	33	47	50
AKD	15	9	7	6
Paper/starch	67	43	31	30
$CaCO_3$	5	5	5	4
Cationic starch	13	10	10	10

Figure 6.26. *Plot of contact angle versus time from sessile drop tests on surface sized fine paper sheets.*

47

6.2.4.2 Cross sectional distribution

The surface coverage of SP+ could thus be correlated with the contact angle but not with the water uptake measured by the Cobb60 method. In the Cobb60 method a water pillar is placed on top of the test paper surface and the pressure may force the water into the porous structure. This means that for a paper to exhibit water resistance in the Cobb60 evaluation, it would need to be hydrophobized also in the interior of the paper matrix. In the surface sizing procedure the SP+/starch mixture is mechanically pressed into the paper sheet while passing through the nip in-between the size press rolls. At the same time the capillary action will bring the liquid into the paper matrix. The subsequent removal of excess water by drying will then create a water flux back to the surface, and it is not well established whether SP+ will go with the flow or stay inside the paper matrix. To evaluate the degree of penetration, cross-sections of paper sheets where low or high amounts of SP+ had been applied were examined with TOF-SIMS. In Figure 6.27 the two cross-sections are shown. It appears as the paper sheet with the lowest water uptake, that is, with higher SP+ dosage, has penetrated into the paper matrix to a larger extent compared to the lower dosage.
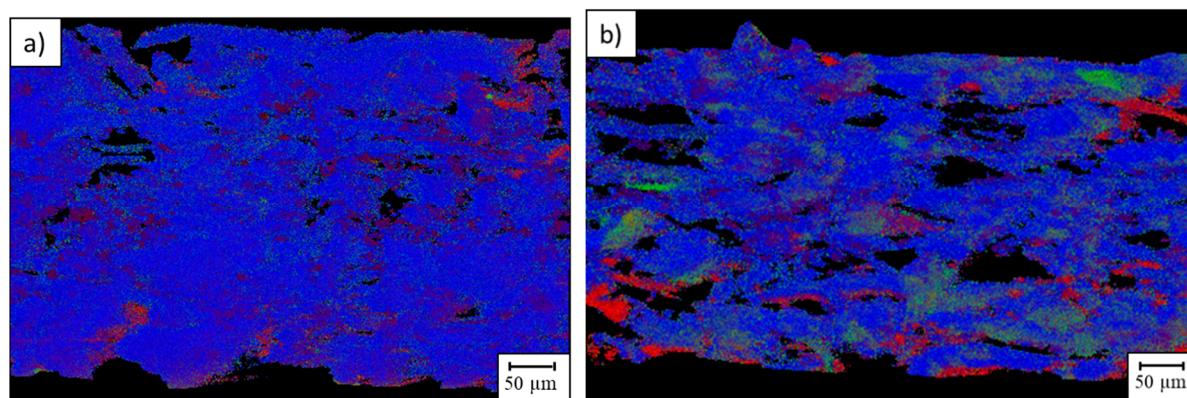

Figure 6.27. *TOF-SIMS images for cross-sections of the surface sized paper at a) low dosage and b) high dosage of SP+. The SP+ distribution is displayed in red color, the AKD distribution in green color and the cellulosic fibers are displayed in blue color.*

6.3 FILM FORMING/PARTICLE RELAXATION

In the papermaking process the subsequent step after surface sizing is drying, in order to remove excess water. The drying at elevated temperatures has empirically been found to influence the hydrophobization effect from the nanoparticles. A sufficiently high drying temperature is needed in order to achieve a proper improvement of water resistance. However, the mechanism behind the temperature effect seems not to have been investigated before. At increased temperature the polymer chains in the particle core will be more flexible and could spread out and stick to the surface, which can be expected to be beneficial. It could also be the film forming process that is crucial. In the case with the formed SP+/starch complexes the aggregates could give rise to a more structured surface that might influence the film formation. Parts of the results discussed here are new, unpublished data that will be included in a future publication.[93]

6.3.1 Film forming on a model surface

In order to study the film forming process and the temperature effect for SP+ and SP-, 0.1 wt. % samples were spin coated on silicon wafers and dried at room temperature or at 80 °C. Figure 6.28 shows how the contact angle for both SP+ and SP- depends on the drying temperature. At a drying temperature above the Tg of the polymer the contact angle is 8-11 degrees higher compared to when dried at room temperature.
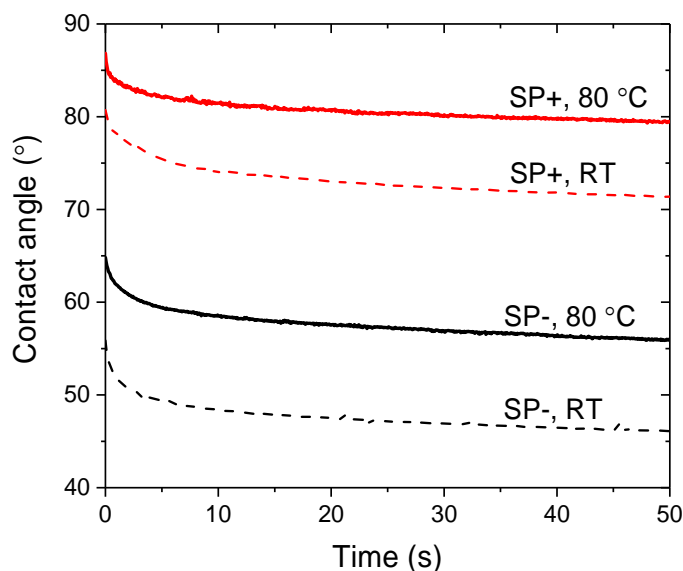

Figure 6.28. *Contact angles for spin coated samples of SP+ and SP- dried at room temperature and at 80 °C.*

Above the Tg, the polymeric core becomes more flexible and a tentative explanation is that when this happens the chains will orient themselves away from the hydrophilic fibers, thus exposing the hydrophobic core towards the paper/air interface. Achieving a more hydrophobic surface after heating above the Tg has been described in the literature for other latex systems.[94] This hypothesis is supported by XPS analyses of SP+ samples dried at room temperature and at 80 °C. The average surface composition differs between the sample dried at room temperature and the sample dried at 80 °C: the amount of nitrogen on the surface was lower for the sample dried at 80 °C. In SP+ it is the hydrophilic stabilizer that contains nitrogen and a decrease in nitrogen content can be interpreted as a phase separation between the stabilizer and the more hydrophobic polymeric particle core.

The phase separation effect was also seen by fluorescence imaging where a fluorophore was incorporated in the polymer chains during the synthesis, thus constituting a part of the hydrophobic core. Images from drop casted SP+ suspensions dried at room temperature and at 80 °C are shown in Figure 6.29. A clear increase in fluorescence can be seen for the sample dried at 80 °C, indicating a difference in surface composition of SP+ upon heat treatment. The mechanism for this change in fluorescence intensity is not clear and it will be investigated in future experiments.
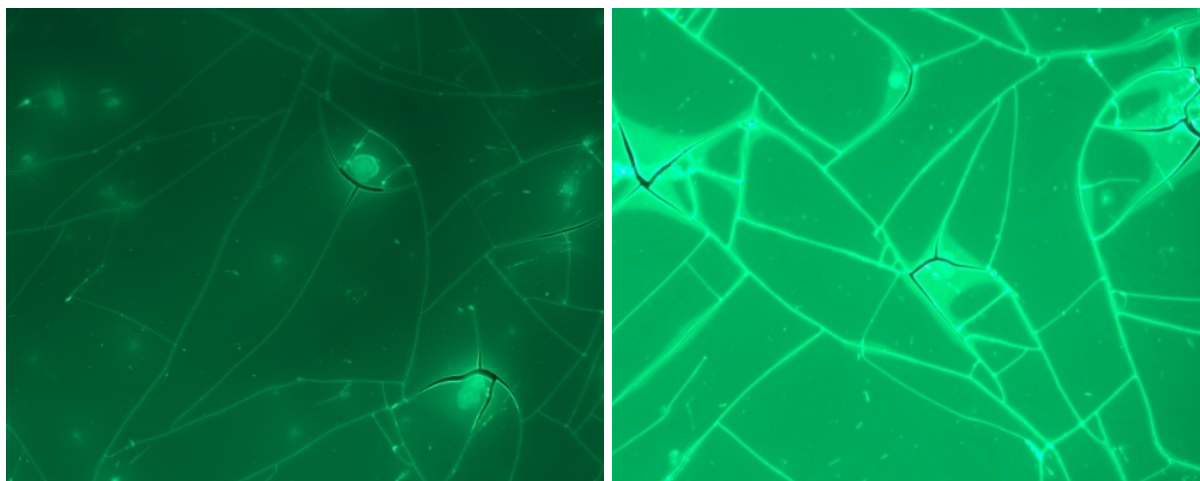
Figure 6.29. *Fluorescence microscopy images of SP+ samples dried at a) room temperature or at b) 80 °C. The same exposure time was employed for both samples.*

6.3.2 Effect of application temperature

In the surface sizing procedure the particle/starch mixture is held at elevated temperature in order to avoid retrogradation of the starch. Since the temperature can affect the flexibility of the polymeric nanoparticles, surface sizing trials were performed at varying temperatures. It was found that the reduction in water uptake was improved when the application temperature was increased (Figure 6.30). With increased temperature the wet pick-up will change due to changes in viscosity and surface tension and these effects were corrected for. However, how the temperature affects the nanoparticles will not be captured by the wet pick-up. With increasing temperature the nanoparticles might become more "sticky" and thus more prone to be retained on the fibers. This improved retention could explain the improved reduction in water uptake with increasing temperature.
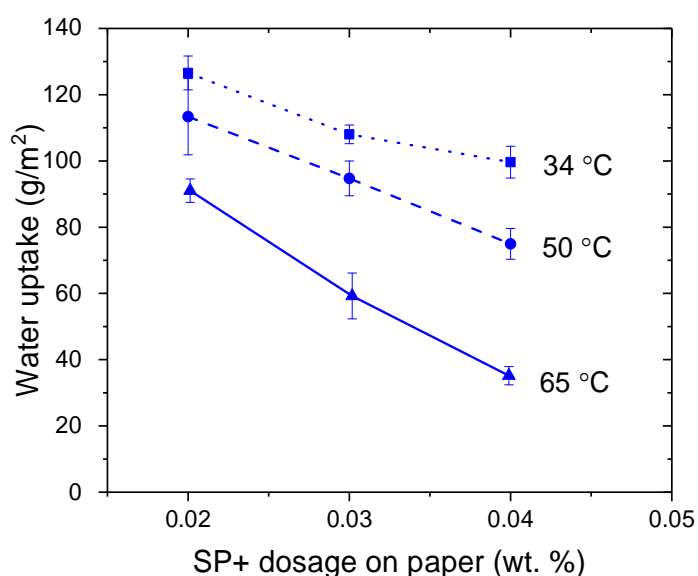

Figure 6.30. *Plot of water uptake versus particle dosage for SP+ at different application temperatures.*

6.3.3 Effect of drying temperature

As discussed above, the contact angle results on spin coated particle suspensions dried either at room temperature or at 80 °C showed that the glass transition temperature plays a significant role for the degree of hydrophobization achieved with the nanoparticles. In a surface sizing trial the drying temperature was varied and the results are shown in Figure 6.31. From this figure it can be seen that when the temperature was below the Tg of the polymer core, i.e. at 40 and 60 °C, the temperature has no effect on the water uptake. When, on the other hand, the Tg is exceeded there is a large improvement in the water uptake reduction. These results correlate well with the contact angle results.
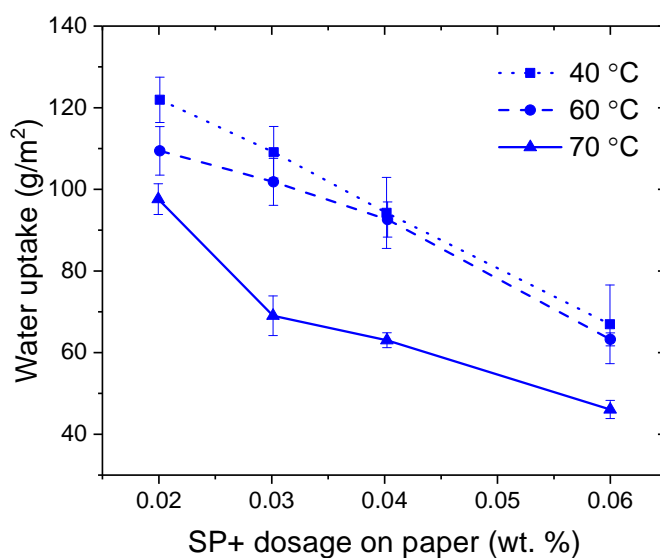

Figure 6.31. *Plot of water uptake versus SP+ dosage for different drying temperatures.*

6.4 TOWARDS A MORE KNOWLEDGE-DRIVEN SURFACE SIZING PROCEDURE

The studies performed in this thesis work were performed with the intention to shed light on the surface sizing procedure. The aim was to gain understanding of which parameters that might influence the process, how to control them and how to take advantage of the interactions that occur due to the nature of the components. Some parameters are fairly easy to adjust in order to optimize the performance while other require more major changes of the formulation or the process. In any case, the understanding gained from this work will hopefully render optimization of the surface sizing process more knowledge-driven. The main findings from the studies are summarized in Figure 6.32.
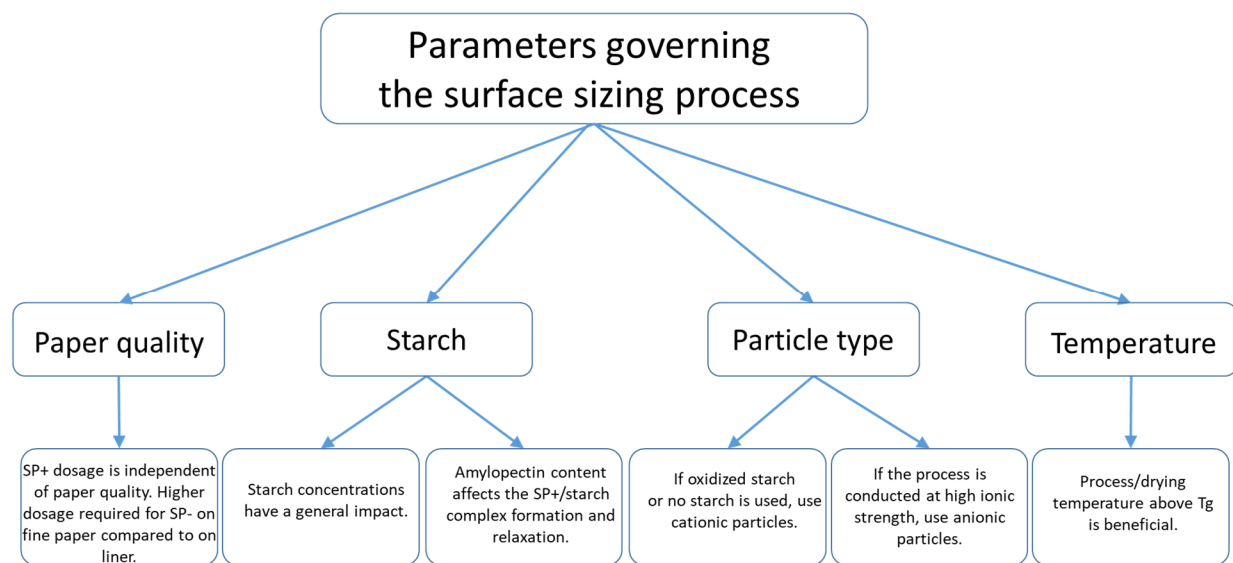

Figure 6.32. *Overview of parameters that influence the surface sizing performance.*

7 CONCLUDING REMARK AND OUTLOOK

In the objectives for this thesis, described in Chapter 2, the four steps in the surface sizing procedure were presented. The aim of the thesis work was to gain deeper understanding of the surface sizing procedure by exploring these four steps. The research work was performed in the chronological order of the surface sizing process, i.e. starting with a study of the colloidal behavior when the surface sizing components were mixed followed by a study of the relaxation kinetics with time, i.e. what may happen during storage. The penetration and possible migration during application of the particle/starch mixture was evaluated by means of water uptake measurements, contact angle determination and TOF-SIMS analysis. The last step in the surface sizing procedure is the drying step, where excess water is removed by increased temperature and the influence of temperature was assessed.

In the first step, the hydrophobic nanoparticle suspension was mixed with a starch solution. The starch used throughout this thesis was an anionic starch, thus having a polyelectrolyte character. Starch is applied on the paper surface mainly to increase the surface strength; however, in this thesis we have shown that the starch can also have an active role in controlling the degree of surface hydrophobization. When cationic particles were mixed with the anionic starch, aggregates were formed and this aggregated state was found to be beneficial for the surface sizing performance. The measured water uptake by a test paper decreased from 80 g/m^2 to 20 g/m^2 just by controlling the aggregate size. At a higher starch to particle ratio the surface charge of the aggregates was reversed to slightly negative and the stabilization mechanism for the aggregates was proposed to be electrosteric stabilization achieved by selective adsorption of the highly branched, high molecular weight amylopectin fraction of the starch solution.

When the colloidal stability was perturbed by an increase in ionic strength, another phenomenon was encountered; the added ions screened the attraction between the cationic particles and the anionic starch, causing a screening-reduced adsorption with a subsequent screening-enhanced adsorption giving larger aggregates when salt was present. At a sufficiently high ionic strength the counter ion effect that is decisive of the colloidal stability was lost and larger flocs were formed due to hydrophobic particle-particle-attraction. In both cases, the increased aggregate/floc formation was found to be detrimental for the surface hydrophobization.

In the study of the colloidal behavior it was found that the initial aggregate size was larger than after an equilibration time, which was attributed to a relaxation of the adsorbed starch chains on the particle surface. At a paper mill, the residence time for the surface sizing mixture can vary and therefore the kinetics of the interactions was studied. The relaxation time was found to be molecular weight dependent; increasing with increasing molecular weight.

In the surface sizing method employed in this thesis work, utilizing a puddle press, the starch/particle mixture was applied on the paper surface by an external pressure which in combination with the capillary forces gave rise to liquid

penetration of the mixture. A study of the distribution of the hydrophobic polymer on and in the test paper was performed with TOF-SIMS. The water uptake evaluated with the Cobb60 method did not correlate with the amount of hydrophobic polymer on the surface. However, when the cross-sections of the surface sized paper sheets were examined it was found that when a larger amount of the hydrophobic polymer was applied, it penetrated deeper into the paper matrix. Penetration into the paper matrix seems thus to be essential in order to achieve low water uptake. Thus, the term *surface sizing* describes the process but does not give a full description of the mechanism.

The last step in the surface sizing procedure is the drying step. In the dryer excess water is removed by heating. The increased temperature has however another important role: to induce polymer relaxation which takes place above the glass transition temperature (Tg). By comparing the water uptake results when paper sheets were dried below or above the Tg the effect was clearly shown; the water uptake was considerably reduced when the drying temperature was raised to above the Tg.

The results discussed in this thesis will hopefully render the surface sizing process more knowledge-driven and easier to optimize.

As is often the case, interesting research results give rise to ideas for new experiments. A more detailed study of the effect of drying on migration and film forming would give further insight into the drying process. An extended colloidal study with different starch types could give valuable information about what starch parameters that are of importance for the colloidal stability and might also shed light on the question about the optimal aggregate size.

ACKNOWLEDGEMENTS

I would also like to thank:

My supervisor Romain Bordes, for your engaged guidance in my project. For the many discussions we have had where time has flown by so fast! For always having time for last minute reviews!

My supervisor Professor Krister Holmberg, for your support and advice, for always taking your time and for your engagement in my project.

My examiner Professor Anders Palmqvist.

Heidi Fagerholm, Kemira R&D global manager, I'm grateful for the time and effort you spend on my project.

Anneli Lepo, Maria Wallgren, Jonas Engström and Michael Persson for being so supportive and engaged in the project as steering group members.

My former supervisor Professor Mats Andersson for initiating the project.

My co-authors Professor Aleksandar Matic and Gregor Trefalt.

Tuan Phan Xuan for assisting me with the MALS and SAXS measurements and for your contributions to the papers as co-author.

Mark Nicholas, for a rewarding collaboration from which I learned a lot! I've very much enjoyed our discussions about science and other important things!

Ann Jakobsson for all administrative help and for nice coffee room chats.

Frida Andersson for all administrative help and nice chats.

Anne Wendel for performing the XPS analyses and nice chats.

Anders Mårtensson for helping me with the SEM analysis.

Annika Altskär for helping me with the TEM analysis.

Stefan Gustavsson, CMAL, for helping me with the SEM analysis for surface roughness.

Tobias Gebäck for the evaluation of the 3D SEM data.

Linda Härdelin, for having the SEC-MALS/RI system in a good shape so I just could jump in with my samples!

Krzysztof Kolman for the discussions about DLS and KWW theory and for being such a great lab company and colleague!

Chaymaa Boujrouf, your internship work gave my project a great start of the film forming studies.

My former roommate Negin Yaghini for all nice discussions about work and life.

Sanna Björkegren, it's always nice to chat with you about work and life in general!

REFERENCES

1. P. Bajpai, *Paper and Paperboard Industry*, Elsevier, USA, 2015.
2. G. Chen, P. Zhu, Y. Kuang, Y. Liu, D. Lin, C. Peng, Z. Wen and Z. Fang, *Applied Surface Science*, 2017, **409**, 45-51.
3. Global production of paper, http://www.forestindustries.se/forest-industry/statistics/international/
4. B.-U. Cho and G. Garnier, *TAPPI Journal*, 2000, **83**, 1-18.
5. J. M. Gess, in *The Sizing of Paper*, ed. J. M. R. Jerome M. Gess, TAPPI Press, Atlanta, Third Edition edn., 2005, ch. 1, pp. 1-7.
6. R. Carceller and A. Juppo, *Paperi ja Puu/Paper and Timber*, 2004, **86**, 161-163.
7. N. Yang and Y. Deng, *Journal of Applied Polymer Science*, 2000, **77**, 2067-2073.
8. T. Lindström and H. O'Brian, *Nordic Pulp and Paper Research Journal*, 1986, **1**, 34-42.
9. M. A. Hubbe, *BioResources*, 2014, **9**, 5782-5783.
10. G. Garnier, J. Wright, L. Godbout and L. Yu, *Colloids and Surfaces A: Physicochemical and Engineering Aspects*, 1998, **145**, 153-165.
11. R. T. Gray and D. S. Rende, in *The Sizing of Paper*, eds. J. M. Gess and J. M. Rodriquez, TAPPI Press, Atlanta, Third edition edn., 2005, ch. 14, pp. 257-286.
12. C. P. Klass, *Pulp and Paper Manufacture* 1991, **17**, 306-322.
13. J. Sajbel, in *The Sizing of Paper*, ed. J. M. R. Jerome M. Gess, Tappi Press, Atlanta, Third edition edn., 2005, ch. 15, pp. 287-300.
14. L. Andersson, C. J. Ridgway and P. A. C. Gane, *Nordic Pulp and Paper Research Journal*, 2013, **28**, 547-558.
15. I. M. T. Moutinho, A. M. Kleen, M. M. L. Figueiredo and P. J. T. Ferreira, *Holzforschung*, 2009, **63**, 282-289.
16. B. W. Ranson, *Pulp and Paper*, 2004, **78**, 50-54.
17. J. Xu and H. Hu, *Journal of Applied Polymer Science*, 2012, **123**, 611-616.
18. X. Wu, Y. Cui, Y. Jing and J. Mossler, *Journal of Bioresourses and Bioproducts*, 2016, **1**, 36-41.
19. C. M. Andersson and L. Järnström, *Appita Journal*, 2006, **59**, 207-212.
20. R. Exner, *Paper Technology*, 2002, **43**, 45-51.
21. I. M. T. Moutinho, P. J. T. Ferreira and M. L. Figueiredo, *BioResources*, 2011, **6**, 4259-4270.
22. P. Wilson, in *The Sizing of Paper*, ed. J. M. R. Jerome M. Gess, Tappi Press, Atlanta, Third edition edn., 2005, ch. 13, pp. 249-256.
23. S. Iwasa, presented in part at the Scientific & Technical Advances in the Internal & Surface Sizing of Paper & Board, Prague, 12-13 December 2001, 2001.
24. J. Anderson, in *Surface Application of Paper Chemicals*, ed. I. T. J. Brander, Springer Science & Business Media, London, 1997, pp. 138-155.
25. J. Gregory, *Advances in Colloid and Interface Science*, 2009, **147-148**, 109-123.
26. C. E. Barnett, *The Journal of Physical Chemistry*, 1942, **46**, 69-75.

27.	R. J. Hunter, Oxford University Press, United States, 2001, ch. 8.2.3, pp. 380-381.
28.	R. J. Hunter, Oxford University Press, United States, 2001, ch. 5.7.3, p. 241.
29.	B. Kronberg, K. Holmberg and B. Lindman, *Surface Chemistry of Surfactants and Polymers*, John Wiley & Sons, Ltd, Chichester, 2014.
30.	T. T. A. o. t. P. a. P. Industry), TAPPI Standard Department, 2013.
31.	J. Israelachvili, *Intermolecular & Surface Forces*, Academic press, United Kingdom, 1991.
32.	K. Grundke, in *Handbook of Applied Surface and Colloid Chemistry*, ed. K. Holmberg, John Wiley & Sons, Ltd, Chichester, 2001, pp. 119-140.
33.	P. Fardim and B. Holmbom, *Applied Surface Science*, 2005, **249**, 393-407.
34.	J. Vickerman, in *ToF-SIMS Surface analysis by mass spectrometry*, eds. J. Vickerman and D. Briggs, IM Publications, Chichester, 2001, pp. 1-40.
35.	A. Benninghoven, B. Hagenhoff and E. Niehuis, *Analytical Chemistry*, 1993, **65**.
36.	K. Kainuma, in *Starch: Chemistry and Technology*, eds. R. L. Whistler, J. N. Bemiller and E. F. Paschall, Academic press, Orlando, FL, 2 edn., 1984, ch. 5, pp. 125-152.
37.	J. J. M. Swinkels, *Starch - Stärke*, 1985, **37**, 1-5.
38.	D. Kuakpetoon and Y. J. Wang, *Starch - Stärke*, 2001, **53**, 211-218.
39.	K. Böckenhoff and W. R. Fischer, *Fresenius' Journal of Analytical Chemistry*, 2001, **371**, 670-674.
40.	R. Wäsche, M. Naito and V. A. Hackley, *Powder Technology*, 2002, **123**, 275-281.
41.	X. Chen, J. Zhang, Z. Yi, Q. Wang, X. Li, F. Bian, J. Wang and Y. Men, *Journal of Coatings Technology Research*, 2011, **8**, 489-496.
42.	J. K. Remmer and D. E. Eklund, *Tappi Journal*, 1992, **75**, 179-184.
43.	D. Kuakpetoon and Y. J. Wang, *Carbohydrate Research*, 2006, **341**, 1896-1915.
44.	C. W. H. John A. Lloyd, *Nordic Pulp & Paper Research Journal*, 1993, **8**.
45.	Y. V. Sood, R. Tyagi, S. Tyagi, P. C. Pande and R. Tondon, *Journal of Scientific and Industrial Research*, 2010, **69**, 300-304.
46.	L. Feng, M. C. Stuart and Y. Adachi, *Advances in Colloid and Interface Science*, 2015, **226**, 101-114.
47.	J. Gregory and S. Barany, *Advances in Colloid and Interface Science*, 2011, **169**, 1-12.
48.	W. L. Yu, F. Bouyer and M. Borkovec, *Journal of Colloid and Interface Science*, 2001, **241**, 392-399.
49.	S. Schwarz, H. M. Buchhammer, K. Lunkwitz and H. J. Jacobasch, *Colloids and Surfaces A: Physicochemical and Engineering Aspects*, 1998, **140**, 377-384.
50.	A. Fuchs and E. Killmann, *Colloid and Polymer Science*, 2001, **279**, 53-60.
51.	G. Carlsson and J. Van Stam, *Nordic Pulp and Paper Research Journal*, 2005, **20**, 192-199.
52.	N. P. Birch and J. D. Schiffman, *Langmuir*, 2014, **30**, 3441-3447.

53. L. Štajner, J. Požar and D. Kovačević, *Colloids and Surfaces A: Physicochemical and Engineering Aspects*, 2015, **483**, 171-180.

54. V. K. La Mer, R. H. Smellie Jr and P. K. Lee, *Journal of Colloid Science*, 1957, **12**, 230-239.

55. L. F. Albright and Knovel, *Albright's Chemical Engineering Handbook*, CRC Press, Boca Raton, 2009.

56. J. B. Rosenholm, J. Nylund and B. Stenlund, *Colloids and Surfaces A: Physicochemical and Engineering Aspects*, 1999, **159**, 209-218.

57. G. Gillies, W. Lin and M. Borkovec, *Journal of Physical Chemistry B*, 2007, **111**, 8626-8633.

58. K. Furusawa, M. Kanesaka and S. Yamashita, *Journal of Colloid And Interface Science*, 1984, **99**, 341-348.

59. Y. Shin, J. E. Roberts and M. M. Santore, *Journal of Colloid and Interface Science*, 2002, **247**, 220-230.

60. F. Mabire, R. Audebert and C. Quivoron, *Journal of Colloid And Interface Science*, 1984, **97**, 120-136.

61. J. Gregory, *Journal of Colloid And Interface Science*, 1973, **42**, 448-456.

62. A. A. Meier-Koll, C. C. Fleck and H. H. Von Grünberg, *Journal of Physics Condensed Matter*, 2004, **16**, 6041-6052.

63. S. Rosenfeldt, A. Wittemann, M. Ballauff, E. Breininger, J. Bolze and N. Dingenouts, *Physical Review E - Statistical, Nonlinear, and Soft Matter Physics*, 2004, **70**, 061403-061401-061403-061410.

64. J. Gregory and I. Sheiham, *British Polymer Journal*, 1974, **6**, 47-59.

65. E. G. M. Pelssers, M. A. C. Stuart and G. J. Fleer, *Colloids and Surfaces*, 1989, **38**, 15-25.

66. Y. Adachi, *Advances in Colloid and Interface Science*, 1995, **56**, 1-31.

67. J. A. De Witt and T. G. M. Van De Ven, *Langmuir*, 1992, **8**, 788-793.

68. R. Ferretti, J. Zhang and J. Buffle, *Colloids and Surfaces A: Physicochemical and Engineering Aspects*, 1997, **121**, 203-215.

69. J. Gregory, *Journal of Colloid And Interface Science*, 1976, **55**, 35-44.

70. J. Zhang, C. Huguenard, C. Scarnecchia, R. Menghetti and J. Buffle, *Colloids and Surfaces A: Physicochemical and Engineering Aspects*, 1999, **151**, 49-63.

71. I. Buffle and G. G. Leppard, *Environmental Science and Technology*, 1995, **29**, 2169-2175.

72. R.S. Anderssen, S.A. Husain and R. J. Loy, *Anziam journal*, 2004, **45**, C800-C816.

73. F. Alvarez, A. Alegra and J. Colmenero, *Physical Review B*, 1991, **44**, 7306-7312.

74. S. L. Shamblin, B. C. Hancock, Y. Dupuis and M. J. Pikal, *Journal of Pharmaceutical Sciences*, 2000, **89**, 417-427.

75. Q. H. Yang, C. J. Qian, H. Li and M. B. Luo, *Physical Chemistry Chemical Physics*, 2014, **16**, 23292-23300.

76. V. Starchenko, M. Müller and N. Lebovka, *Journal of Physical Chemistry B*, 2012, **116**, 14961-14967.

77. E. Leontidis, *Current Opinion in Colloid and Interface Science*, 2002, **7**, 81-91.

78.   T. López-León, A. B. Jódar-Reyes, D. Bastos-González and J. L. Ortega-Vinuesa, *Journal of Physical Chemistry B*, 2003, **107**, 5696-5708.

79.   T. Oncsik, G. Trefalt, Z. Csendes, I. Szilagyi and M. Borkovec, *Langmuir*, 2014, **30**, 733-741.

80.   G. Trefalt, I. Szilagyi, G. Téllez and M. Borkovec, *Langmuir*, 2017, **33**, 1695-1704.

81.   A. S. Michaels, *Industrial & Engineering Chemistry*, 1954, **46**, 1485-1490.

82.   H. G. M. van de Steeg, A. de Keizer, M. A. C. Stuart and B. H. Bijsterbosch, *Colloids and Surfaces A: Physicochemical and Engineering Aspects*, 1993, **70**, 91-103.

83.   H. G. M. van de Steeg, M. A. C. Stuart, A. de keizer and B. H. Bijsterbosch, *Langmuir*, 1992, **8**, 2538-2546.

84.   T. Radeva, V. Milkova and I. Petkanchin, *Colloids and Surfaces A: Physicochemical and Engineering Aspects*, 2002, **209**, 227-233.

85.   D. Bauer, E. Killmann and W. Jaeger, *Colloid and Polymer Science*, 1998, **276**, 698-708.

86.   T. Cosgrove, T. M. Obey and B. Vincent, *Journal of Colloid And Interface Science*, 1986, **111**, 409-418.

87.   B. C. Bonekamp, R. Hidalgo Alvarez, F. J. De Las Nieves and B. H. Busterbosch, *Journal of Colloid And Interface Science*, 1987, **118**, 366-371.

88.   E. Killmann, D. Bauer, A. Fuchs, O. Portenlänger, R. Rehmet and O. Rustemeier, in *Progress in Colloid and Polymer Science*, 1998, vol. 111, pp. 135-143.

89.   I. M. T. Moutinho, P. J. T. Ferreira and M. L. Figueiredo, *Industrial and Engineering Chemistry Research*, 2007, **46**, 6183-6188.

90.   B. Brungardt, Proceedings of the 1997 83rd Annual Meeting of the Technical Section of Canadian Pulp and Paper Association, 1997.

91.   J. Lipponen, J. Grön, S. E. Bruun and T. Laine, *Journal of Pulp and Paper Science*, 2004, **30**, 82-90.

92.   F. Iselau, M. Nicholas, A. Martinelli, K. Holmberg and R. Bordes, *To be published*.

93.   F. Iselau, C. Boujrouf, K. Holmberg and R. Bordes, *To be published*.

94.   L. Carlsson, A. Fall, I. Chaduc, L. Wågberg, B. Charleux, E. Malmström, F. D'Agosto, M. Lansalot and A. Carlmark, *Polymer Chemistry*, 2014, **5**, 6076-6086.